nature communications

Article

https://doi.org/10.1038/s41467-024-51164-5

Lymphotoxin limits Foxp3^{+} regulatory T cell development from Foxp3^{lo} precursors via IL-4 signaling

Received: 26 September 2023

Accepted: 31 July 2024

Published online: 14 August 2024

Check for updates

Alexia Borelli[1], Jérémy C. Santamaria[1], Cloé Zamit[1], Cécile Apert[2,3], Jessica Chevallier[1], Philippe Pierre[1], Rafael J. Argüello[1], Lionel Spinelli[1] & Magali Irla[1]

Regulatory T cells (T_{reg}) are critical players of immune tolerance that develop in the thymus via two distinct developmental pathways involving CD25^{+}Foxp3^{-} and CD25^{-}Foxp3^{lo} precursors. However, the mechanisms regulating the recently identified Foxp3^{lo} precursor pathway remain unclear. Here, we find that the membrane-bound lymphotoxin $\alpha_1\beta_2$ ($LT\alpha_1\beta_2$) heterocomplex is upregulated during T_{reg} development upon TCR/CD28 and IL-2 stimulation. We show that *Lta* expression limits the maturational development of T_{reg} from Foxp3^{lo} precursors by regulating their proliferation, survival, and metabolic profile. Transgenic reporter mice and transcriptomic analyses further reveal that medullary thymic epithelial cells (mTEC) constitute an unexpected source of IL-4. We demonstrate that $LT\alpha_1\beta_2$-lymphotoxin β receptor-mediated interactions with mTEC limit T_{reg} development by down-regulating IL-4 expression in mTEC. Collectively, our findings identify the lymphotoxin axis as the first inhibitory checkpoint of thymic T_{reg} development that fine-tunes the Foxp3^{lo} T_{reg} precursor pathway by limiting IL-4 availability.

Regulatory T cells (T_{reg}) constitute a subset of CD4^{+} T cells that specifically express the transcription factor Foxp3 and CD25, also known as IL-2Rα. Naturally occurring CD25^{+}Foxp3^{+} T_{reg} critically prevent autoimmune and inflammatory disorders by maintaining self-tolerance through the suppression of autoreactive T cells that have escaped thymic selection. The majority of CD25^{+}Foxp3^{+} T_{reg} emerge in the thymus from 3 days after birth[1]. In particular, medullary thymic epithelial cells (mTEC) contribute to T_{reg} development by expressing MHC class II and CD80/86 molecules as well as a broad range of self-antigens[2–4]. T_{reg} development follows a "two-step" model in the thymic medulla[5–7]. The first step is driven by the stimulation of the T-cell receptor (TCR) and of CD28 in developing CD4^{+} single-positive (SP) thymocytes, leading to the generation of CD25^{+}Foxp3^{-} precursors (CD25^{+} T_{reg}P)[5,6,8]. TCR and CD28 signals govern the expression of tumor-necrosis factor receptor (TNFR) members, GITR and OX40, which promote CD25 expression[9]. The second step is driven by γ-chain cytokines, in particular IL-2 and IL-15, that convert CD25^{+} T_{reg}P into CD25^{+}Foxp3^{+} mature T_{reg}[5]. In addition to Foxp3 upregulation, IL-2 also modulates GITR and OX40 expression in mature T_{reg}[10]. IL-2 was found to be provided by autoreactive CD4^{+} SP thymocytes[11], whereas IL-15 is produced by mTEC[12]. More recently, a second CD25^{-}Foxp3^{lo} precursor (Foxp3^{lo} T_{reg}P), lacking CD25 and expressing low levels of Foxp3, was identified[13]. Similarly to CD25^{+} T_{reg}P, this precursor has the ability to generate CD25^{+}Foxp3^{+} mature T_{reg} upon intrathymic transfer[14,15]. The differentiation of Foxp3^{lo} T_{reg}P into mature T_{reg} also follows the "two-step" model[9,15]. Although Foxp3^{lo} T_{reg}P make a substantial contribution to the mature T_{reg} pool, the mechanisms controlling this recently identified developmental pathway remain elusive. Peripheral Foxp3^{+} T_{reg} were shown to express the membrane-bound lymphotoxin $\alpha_1\beta_2$ ($LT\alpha_1\beta_2$) heterocomplex, belonging to the TNF superfamily, which

[1]Aix-Marseille University, CNRS, INSERM, CIML, Centre d'Immunologie de Marseille-Luminy, Turing Centre for Living Systems, Marseille, France. [2]Toulouse Institute for Infectious and Inflammatory Diseases (Infinity), INSERM UMR1291—CNRS UMR5051—University Toulouse III, Toulouse, France. [3]Present address: Microenvironment & Immunity Unit, Institut Pasteur, Paris, France. e-mail: Magali.Irla@inserm.fr

interacts with its unique cognate LTβ receptor (LTβR)[16–18]. However, it remains unknown whether $LT\alpha_1\beta_2$ expression is induced in thymic T_{reg} and whether it controls their generation.

Here, we show that $LT\alpha_1\beta_2$ gradually increases during the "two-step" model of thymic T_{reg} development. Its upregulation depends on TCR/CD28 stimulation in $CD25^+$ and $Foxp3^{lo}$ $T_{reg}P$, and on IL-2 stimulation in $CD25^+Foxp3^+$ mature T_{reg}. Interestingly, we observed an increased development of $Foxp3^{lo}$ $T_{reg}P$ and mature T_{reg} in $Foxp3^{eGFP}$x*Lta*$^{-/-}$ mice, indicating that *Lta* negatively regulates $CD25^+Foxp3^+$ T_{reg} generation from $Foxp3^{lo}$ $T_{reg}P$. This phenotype was associated with an increased proliferation and survival of $Foxp3^{lo}$ $T_{reg}P$ and mature T_{reg}, as well as an altered metabolic profile. Strikingly, the maturational development of $Foxp3^{lo}$ $T_{reg}P$ and $CD25^+Foxp3^+$ T_{reg} increased in these mice. We show that IL-4 stimulation substantially promotes the conversion of $Foxp3^{lo}$ $T_{reg}P$ into $CD25^+Foxp3^+$ mature T_{reg} and that mTEC constitute an unexpected source of IL-4. We further demonstrate that the $LT\alpha_1\beta_2$-LTβR axis negatively regulates the generation of $CD25^+Foxp3^+$ T_{reg} by limiting IL-4 expression in mTEC. Altogether, this study reveals that $LT\alpha_1\beta_2$-LTβR interactions with mTEC fine-tunes the $Foxp3^{lo}$ $T_{reg}P$ developmental pathway in an IL-4-dependent manner.

Results

$LT\alpha_1\beta_2$ expression is upregulated during thymic T_{reg} development

To characterize $LT\alpha_1\beta_2$ expression during thymic T_{reg} development, we used *Rag2*^{GFP}x*Foxp3*$^{Thy1.1}$ mice expressing the green fluorescent protein (GFP) and the membrane-bound Thy1.1 under the control of *Rag2* and *Foxp3* promoters, respectively[19,20]. These mice allowed us to discriminate newly generated thymocytes (*Rag2*$^{GFP+}$) from more mature T_{reg} that have been retained within the thymus or have recirculated from the periphery (*Rag2*$^{GFP-}$)[21–23]. Among *Rag2*$^{GFP+}$ thymocytes, we identified newly produced $CD4^+$ SP thymocyte subsets: $CD4^+$ T_{conv} ($CD25^-Foxp3^-$), $CD25^+$ $T_{reg}P$ ($CD25^+Foxp3^-$), $Foxp3^{lo}$ $T_{reg}P$ ($CD25^-Foxp3^{lo}$) and mature T_{reg} ($CD25^+Foxp3^+$) (Fig. 1a). The expression of the membrane-bound $LT\alpha_1\beta_2$ heterocomplex, detected using the soluble LTβR-Fc receptor, was higher in $CD25^+$ $T_{reg}P$ and $Foxp3^{lo}$ $T_{reg}P$ compared to $CD4^+$ T_{conv} (Fig. 1b, c). This expression was even further increased in newly produced $CD25^+Foxp3^+$ T_{reg}. In contrast, the

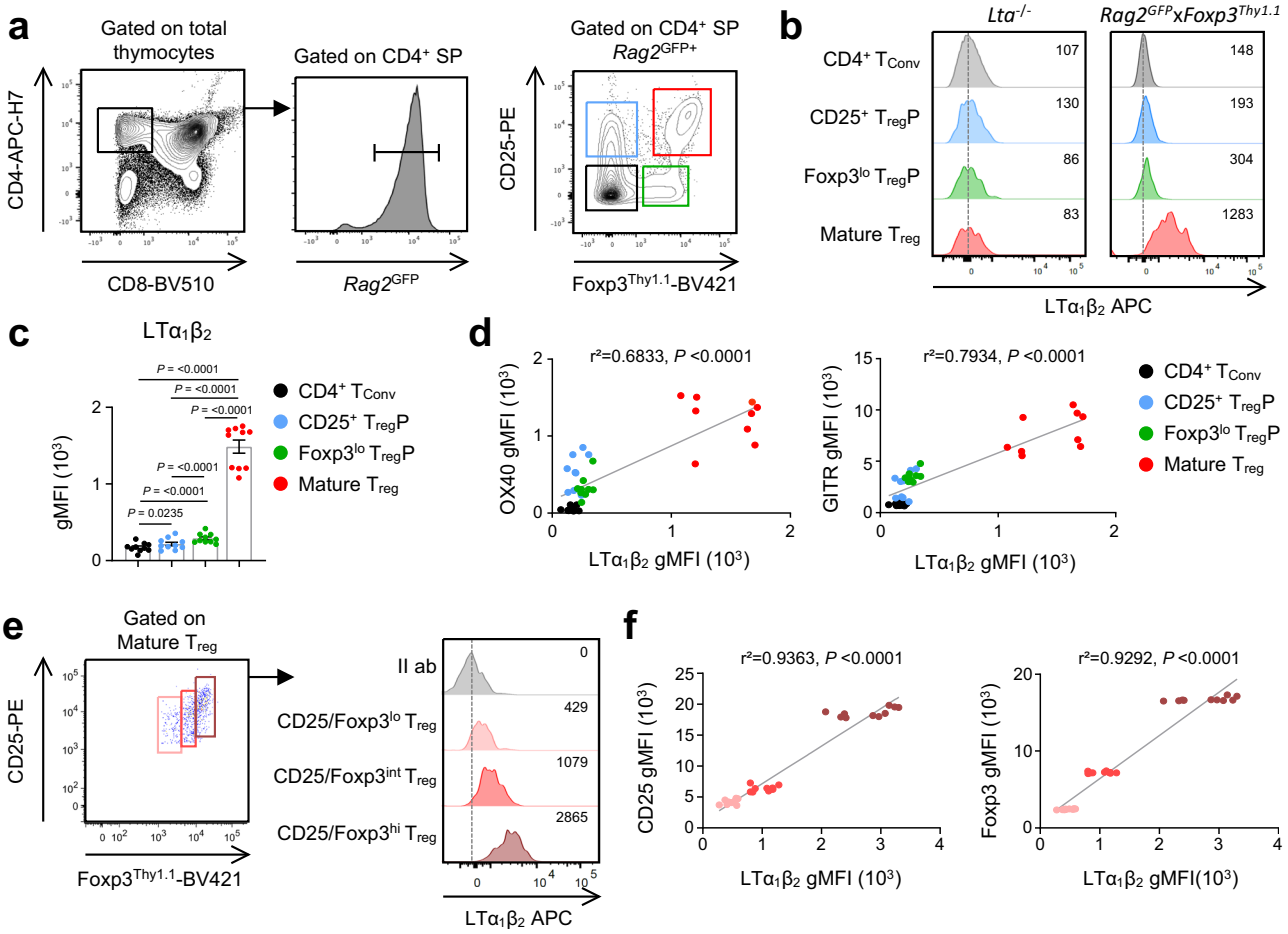

Fig. 1 | Membrane-bound $LT\alpha_1\beta_2$ expression increases during thymic T_{reg} development concomitantly with OX40 and GITR. a Gating strategy used to analyze conventional $CD4^+$ SP thymocytes ($CD4^+$ T_{conv}, $CD4^+CD8^-$Rag2^{GFP+} $CD25^-Foxp3^-$; black), $CD25^+$ $T_{reg}P$ ($CD4^+CD8^-$Rag2$^{GFP+}CD25^+Foxp3^-$; blue), $Foxp3^{lo}$ $T_{reg}P$ ($CD4^+CD8^-$Rag2$^{GFP+}CD25^-Foxp3^{lo}$; green), and mature T_{reg} ($CD4^+CD8^-$Rag2^{GFP+} $CD25^+Foxp3^+$; red) in *Rag2*^{GFP}x*Foxp3*$^{Thy1.1}$ mice by flow cytometry. **b** Representative histograms and quantification of membrane-bound $LT\alpha_1\beta_2$ expression, detected using the soluble LTβR-Fc receptor, in $CD4^+$ T_{conv}, $CD25^+$ $T_{reg}P$, $Foxp3^{lo}$ $T_{reg}P$, and mature T_{reg} from *Rag2*^{GFP}x*Foxp3*$^{Thy1.1}$ mice and *Lta*$^{-/-}$ controls. **c** Geometric MFI (gMFI) of $LT\alpha_1\beta_2$ expression in thymic T_{reg} subsets (n = 10 from three independent experiments. **d** Correlation between $LT\alpha_1\beta_2$ and OX40 or GITR expression in thymic T_{reg} subsets (n = 9 from three independent experiments). **e** Gates represent the expression spectrum of CD25 and Foxp3 (left) in mature T_{reg} that were analyzed for $LT\alpha_1\beta_2$ expression (right). The gray histogram corresponds to mature T_{reg} stained with only the secondary antibody. **f** Correlation between $LT\alpha_1\beta_2$ and CD25 (left) or Foxp3 expression (right) in each gates (n = 10 from three independent experiments). Correlations were calculated using the parametric two-tailed Pearson correlation test for (**d**) and the non-parametric two-tailed Spearman correlation test for (**f**). Error bars show mean ± SEM, *p < 0.05, **p < 0.01 and ****p < 0.0001 using one-way ANOVA. Source data are provided as a Source Data File.

soluble LTβR-Fc receptor did not bind to thymic T_{reg} subsets from *Lta*$^{-/-}$ mice (Fig. 1b). We also used the differential expression of CCR6, which discriminates between newly produced T_{reg} (CCR6$^-$) and recirculating T_{reg} (CCR6$^+$) in the thymus[4] and confirmed *Lta* and *Ltb* upregulation during T_{reg} development using Foxp3^{eGFP} reporter mice, in which an enhanced GFP reporter construct was introduced into the *Foxp3* locus (Supplementary Fig. 1). Interestingly, the gradual upregulation of $LT\alpha_1\beta_2$ expression during T_{reg} development correlated with that of OX40 (*Tnfrsf4*) and GITR (*Tnfrsf18*) (Fig. 1d and Supplementary Fig. 1c). Furthermore, cells with the highest CD25 expression also had the highest Foxp3 expression in newly produced mature T_{reg} and $LT\alpha_1\beta_2$ level tightly correlated with CD25 and Foxp3 levels (Fig. 1e,f). These results show that $LT\alpha_1\beta_2$ is gradually upregulated during T_{reg} development in the thymus.

$LT\alpha_1\beta_2$ is upregulated by instructive signals of the "two-step model" of T_{reg} development

Since we observed a tight correlation between $LT\alpha_1\beta_2$ and Foxp3 levels, we then asked whether $LT\alpha_1\beta_2$ upregulation could be related to TCR stimulation. To address this question, we used the transcription factor Nur77 as a reliable readout of TCR signal strength[24] and found a significant positive correlation between $LT\alpha_1\beta_2$ and Nur77 in CD25$^+$ T_{reg}P, Foxp3^{lo} T_{reg}P and mature T_{reg} (Fig. 2a and Supplementary Fig. 2a). We also analyzed $LT\alpha_1\beta_2$ expression in T_{reg} subsets stimulated in vitro with increasing doses of anti-CD3ε monoclonal antibody, which upregulated $LT\alpha_1\beta_2$ expression in both CD25$^+$ T_{reg}P and Foxp3^{lo} T_{reg}P (Fig. 2b and Supplementary Fig. 2b). In contrast, CD3ε stimulation was unable to upregulate $LT\alpha_1\beta_2$ expression in mature T_{reg}. We next assessed the effect of CD28 costimulation on $LT\alpha_1\beta_2$ expression. To this end, we used *Cd28*$^{-/-}$ mice, which showed decreased frequencies and numbers of CD25$^+$ T_{reg}P, Foxp3^{lo} T_{reg}P, and mature T_{reg} (Supplementary Fig. 3a). Similarly to OX40 and GITR, $LT\alpha_1\beta_2$ was reduced in these cells (Fig. 2c and Supplementary Fig. 3b,c), indicating that CD28 costimulation is implicated in $LT\alpha_1\beta_2$ upregulation in T_{reg} subsets.

Given that IL-2 and IL-15 are crucial for the conversion of T_{reg}P into CD25$^+$Foxp3$^+$ mature T_{reg}[5,10,25], we hypothesized that these cytokines could also be implicated in $LT\alpha_1\beta_2$ upregulation. To address their respective contribution, we used *Il2*^{KO} or *Il15*^{KO} mice backcrossed with *Rag2*^{GFP}x*Foxp3*$^{Thy1.1}$ mice to analyze newly generated T_{reg}. In contrast to *Il15*^{KO}x*Rag2*^{GFP}x*Foxp3*$^{Thy1.1}$ (*Il15*$^{-/-}$) mice (Fig. 2d), $LT\alpha_1\beta_2$ expression was strongly altered in mature T_{reg} from *Il2*^{KO}x*Rag2*^{GFP}x*Foxp3*$^{Thy1.1}$ (*Il2*$^{-/-}$) mice (Fig. 2e). Because thymic IL-2 is important for T_{reg} development and survival[13,26], we next sought to demonstrate that IL-2 directly regulates $LT\alpha_1\beta_2$ expression in mature T_{reg}. To this end, purified CD25$^+$ T_{reg}P, Foxp3^{lo} T_{reg}P and mature T_{reg} were stimulated in vitro with increasing doses of IL-2. Interestingly, $LT\alpha_1\beta_2$ was upregulated in an IL-2 dose-dependent manner in mature T_{reg} (Fig. 2f and Supplementary Fig. 2c). Altogether, these results show that $LT\alpha_1\beta_2$ upregulation is initially induced by TCR/CD28 signals in T_{reg}P and further upregulated by IL-2 stimulation in mature T_{reg} and thus, controlled by the signals of the "two-step model" of T_{reg} development.

$LT\alpha_1\beta_2$ limits T_{reg} generation through the Foxp3^{lo} T_{reg}P developmental pathway

To test whether *Lta* could be implicated in T_{reg} development, we backcrossed *Lta*$^{-/-}$ mice with Foxp3^{eGFP} mice (Foxp3^{eGFP}x*Lta*$^{-/-}$ mice), in which membrane-bound $LT\alpha_1\beta_2$ expression is fully abolished[18]. Remarkably, in contrast to CD25$^+$ T_{reg}P, frequencies and numbers of Foxp3^{lo} T_{reg}P and mature T_{reg} were substantially higher in 6-week-old Foxp3^{eGFP}x*Lta*$^{-/-}$ mice compared to Foxp3^{eGFP} controls (Fig. 3a, b). This phenotype was also observed in the thymus of 3-day-old neonates, indicating that *Lta* regulates the development of Foxp3^{lo} T_{reg}P and mature T_{reg} from their emergence (Fig. 3c, d). Moreover, 4-month-old adult Foxp3^{eGFP}x*Lta*$^{-/-}$ mice also showed an increased representation of these cells, suggesting that *Lta* controls T_{reg} development throughout the lifespan. Since we previously reported an enhanced clonal deletion of CD4$^+$ T_{conv} in *Lta*$^{-/-}$ mice[27], we further analyzed the impact of *Lta* specifically on developing cells within the T_{reg} lineage (Supplementary Fig. 4a). In accordance with the increased cellularity of Foxp3^{lo} T_{reg}P and mature T_{reg} (Fig. 3a–d), frequencies of these cells were enhanced in the T_{reg} lineage of Foxp3^{eGFP}x*Lta*$^{-/-}$ mice (Supplementary Fig. 4a). In line with this phenotype, frequencies and numbers of Ki67$^+$ proliferating cells were increased in Foxp3^{lo} T_{reg}P and mature T_{reg} subsets of Foxp3^{eGFP}x*Lta*$^{-/-}$ mice (Fig. 3e). Moreover, frequencies of annexin V$^+$ were reduced in Foxp3^{lo} T_{reg}P from Foxp3^{eGFP}x*Lta*$^{-/-}$ mice (Fig. 3f). Lower levels of the pro-apoptotic protein BIM, which is required for the apoptosis of autoreactive thymocytes[28,29], were also observed in Foxp3^{lo} T_{reg}P and mature T_{reg} of these mice (Fig. 3g). In contrast, Ki67$^+$ proliferating cells were slightly increased while annexin V$^+$ cells and BIM levels were unchanged in CD25$^+$ T_{reg}P (Supplementary Fig. 4c–e). Thus, the increase of Foxp3^{lo} T_{reg}P and mature T_{reg} in Foxp3^{eGFP}x*Lta*$^{-/-}$ mice likely relies on enhanced proliferation and survival.

Given that cells of the T_{reg} lineage are heterogeneous, we further analyzed their maturational state in Foxp3^{eGFP}x*Lta*$^{-/-}$ mice using a multiparametric flow cytometry analysis with developmental markers (Fig. 3h). We performed an unsupervised clustering that revealed a high maturational heterogeneity within the T_{reg} lineage (Fig. 3i). Cell subsets were classified according to the relative expression of the maturational markers used (Fig. 3j). Subsets 1–5 corresponded to CD25$^+$ T_{reg}P, subsets 6–8 to Foxp3^{lo} T_{reg}P and subsets 9–10 to mature T_{reg} (Fig. 3i, j). In Foxp3^{eGFP}x*Lta*$^{-/-}$ mice, CD25$^+$ T_{reg}P subsets (clusters 1–4) were under-represented, while two immature Foxp3^{lo} T_{reg}P subsets (clusters 6,7) were unchanged (Fig. 3k). In contrast, the Foxp3^{lo} T_{reg}P cluster 8 expressing high levels of H2K^b and Qa2 and low levels of CD69 and CD24, likely corresponding to more mature transitional Foxp3^{lo} T_{reg}P, was over-represented in Foxp3^{eGFP}x*Lta*$^{-/-}$ mice. Strikingly, we found an increased representation of mature T_{reg} subsets (clusters 9, 10) in Foxp3^{eGFP}x*Lta*$^{-/-}$ mice. These results reveal a bias in the T_{reg} maturational development via Foxp3^{lo} T_{reg}P in Foxp3^{eGFP}x*Lta*$^{-/-}$ mice.

Because the $LT\alpha_1\beta_2$-LTβR axis controls thymic medulla organization[17,30], we analyzed the contribution of non-hematopoietic cells in T_{reg} development by generating bone marrow (BM) chimeras in which lethally irradiated CD45.2 WT or *Lta*$^{-/-}$ recipients were reconstituted with CD45.1 Foxp3^{eGFP} BM cells (Supplementary Fig. 5a). Six weeks later, similar frequencies and numbers of CD25$^+$ T_{reg}P, Foxp3^{lo} T_{reg}P, and mature T_{reg} were observed in the thymus of WT and *Lta*$^{-/-}$ recipients (Supplementary Fig. 5b), indicating that the stromal environment of *Lta*$^{-/-}$ mice is unlikely implicated in the enhanced T_{reg} development. Given that *Lta* is expressed by hematopoietic cells[17], we next wondered whether a partial reintroducion of WT BM cells with *Lta*$^{-/-}$ BM cells could be sufficient to reverse the phenotype observed in *Lta*$^{-/-}$ mice. To this end, we generated mixed BM chimeras in which lethally irradiated CD45.1/2 WT recipients were reconstituted with BM cells from either CD45.1 Foxp3^{eGFP} or Foxp3^{eGFP}x*Lta*$^{-/-}$ mice in competition with CD45.2 WT BM cells (Fig. 4a). Six weeks later, as opposed to CD25$^+$ T_{reg}P, we found increased frequencies of Foxp3^{lo} T_{reg}P and mature T_{reg} in Foxp3^{eGFP}x*Lta*$^{-/-}$ + WT → WT chimeras (Fig. 4b). Moreover, we observed enhanced frequencies of Foxp3^{lo} T_{reg}P and mature T_{reg} by specifically analyzing cells of the T_{reg} lineage (Fig. 4c). In line with these observations, we found slightly decreased frequencies of Ki67$^+$ CD25$^+$ T_{reg}P while Foxp3^{lo} T_{reg}P proliferation increased (Fig. 4d). We next analyzed the maturational state of cells from the T_{reg} lineage using a multiparametric flow cytometry analysis (Fig. 4e). We performed an unsupervised clustering that revealed

https://doi.org/10.1038/s41467-024-51164-5

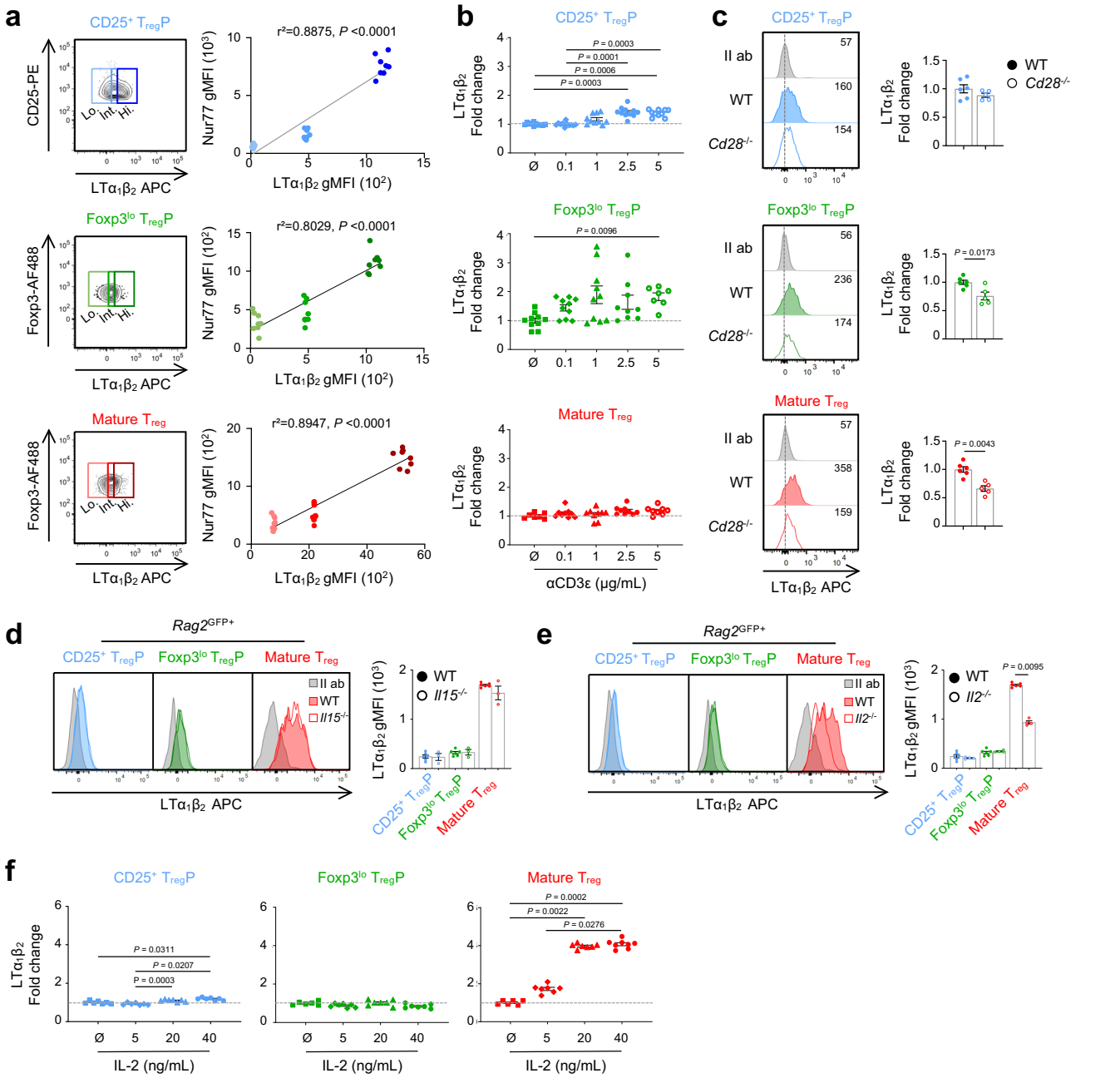

Fig. 2 | LTα$_1$β$_2$ expression is upregulated during thymic T$_{reg}$ development by TCR/CD28 and IL-2 signals. a Correlation between LTα$_1$β$_2$ and Nur77 expression in CD25$^+$ T$_{reg}$P (upper panel), Foxp3^{lo} T$_{reg}$P (middle panel), and CD25$^+$Foxp3$^+$ mature T$_{reg}$ (lower panel) in CCR6$^-$ cells (n = 8 from two independent experiments). **b** Fold change in LTα$_1$β$_2$ expression measured in purified CCR6$^-$ CD25$^+$ T$_{reg}$P, Foxp3^{lo} T$_{reg}$P and mature T$_{reg}$ stimulated with 0.1 μg/mL (diamond, n = 11 for CD25$^+$ T$_{reg}$P, n = 10 for Foxp3^{lo} T$_{reg}$P and n = 9 for mature T$_{reg}$), 1 μg/mL (triangle, n = 10 for CD25$^+$ T$_{reg}$P, n = 10 for Foxp3^{lo} T$_{reg}$P and n = 9 for mature T$_{reg}$), 2.5 μg/mL (filled circle, n = 11 for CD25$^+$ T$_{reg}$P, n = 9 for Foxp3^{lo} T$_{reg}$P and n = 9 for mature T$_{reg}$) or with 5 μg/mL anti-CD3 antibodies (open circle, n = 10 for CD25$^+$ T$_{reg}$P, n = 7 for Foxp3^{lo} T$_{reg}$P and n = 8 for mature T$_{reg}$). Unstimulated cells (square, n = 11 for CD25$^+$ T$_{reg}$P, n = 10 for Foxp3^{lo} T$_{reg}$P, and n = 7 for mature T$_{reg}$) were used as controls. Data are pooled from two independent experiments. **c** Representative histograms of LTα$_1$β$_2$ expression (left) and fold change (right) in CCR6$^-$ CD25$^+$ T$_{reg}$P, Foxp3^{lo} T$_{reg}$P, and mature T$_{reg}$ from WT (n = 6) and *Cd28*$^{-/-}$ (n = 5) mice. Data are pooled from two independent experiments. **d**, **e** Representative histograms (left) and quantification (right) of LTα$_1$β$_2$ expression levels in CD25$^+$ T$_{reg}$P, Foxp3^{lo} T$_{reg}$P and mature T$_{reg}$ from littermate controls (n = 6), *Il15*^{KO}x*Rag2*^{GFP}x*Foxp3*$^{Thy1.1}$ (*Il15*$^{-/-}$) (n = 3) **(d)** or *Il2*^{KO} x*Rag2*^{GFP}x*Foxp3*$^{Thy1.1}$(*Il2*$^{-/-}$) (n = 4) **(e)** mice. The gray histogram corresponds to mature T$_{reg}$ stained with only the secondary antibody. Data are pooled from two independent experiments. **f** Fold change in LTα$_1$β$_2$ expression in purified CCR6$^-$ CD25$^+$ T$_{reg}$P, Foxp3^{lo} T$_{reg}$P and mature T$_{reg}$ stimulated with 5 ng/mL (diamond, n = 7 for CD25$^+$ T$_{reg}$P, n = 7 for Foxp3^{lo} T$_{reg}$P and n = 7 for mature T$_{reg}$), 20 ng/mL (triangle, n = 7 for CD25$^+$ T$_{reg}$P, n = 7 for Foxp3^{lo} T$_{reg}$P and n = 7 for mature T$_{reg}$), 40 ng/mL IL-2 (circle, n = 7 for CD25$^+$ T$_{reg}$P, n = 7 for Foxp3^{lo} T$_{reg}$P and n = 7 for mature T$_{reg}$) or unstimulated (square, n = 7 for CD25$^+$ T$_{reg}$P, n = 6 for Foxp3^{lo} T$_{reg}$P and n = 6 for mature T$_{reg}$). Data are pooled from two independent experiments (n = 8). Correlations were calculated using the non-parametric two-tailed Spearman correlation test for (**a**). Error bars show mean ± SEM, *p < 0.05, **p < 0.01, and ***p < 0.001 using Kruskal–Wallis test for (**b**, **f**) and unpaired two-tailed Mann–Whitney U test for (**c**–**e**). Source data are provided as a Source Data File.

https://doi.org/10.1038/s41467-024-51164-5

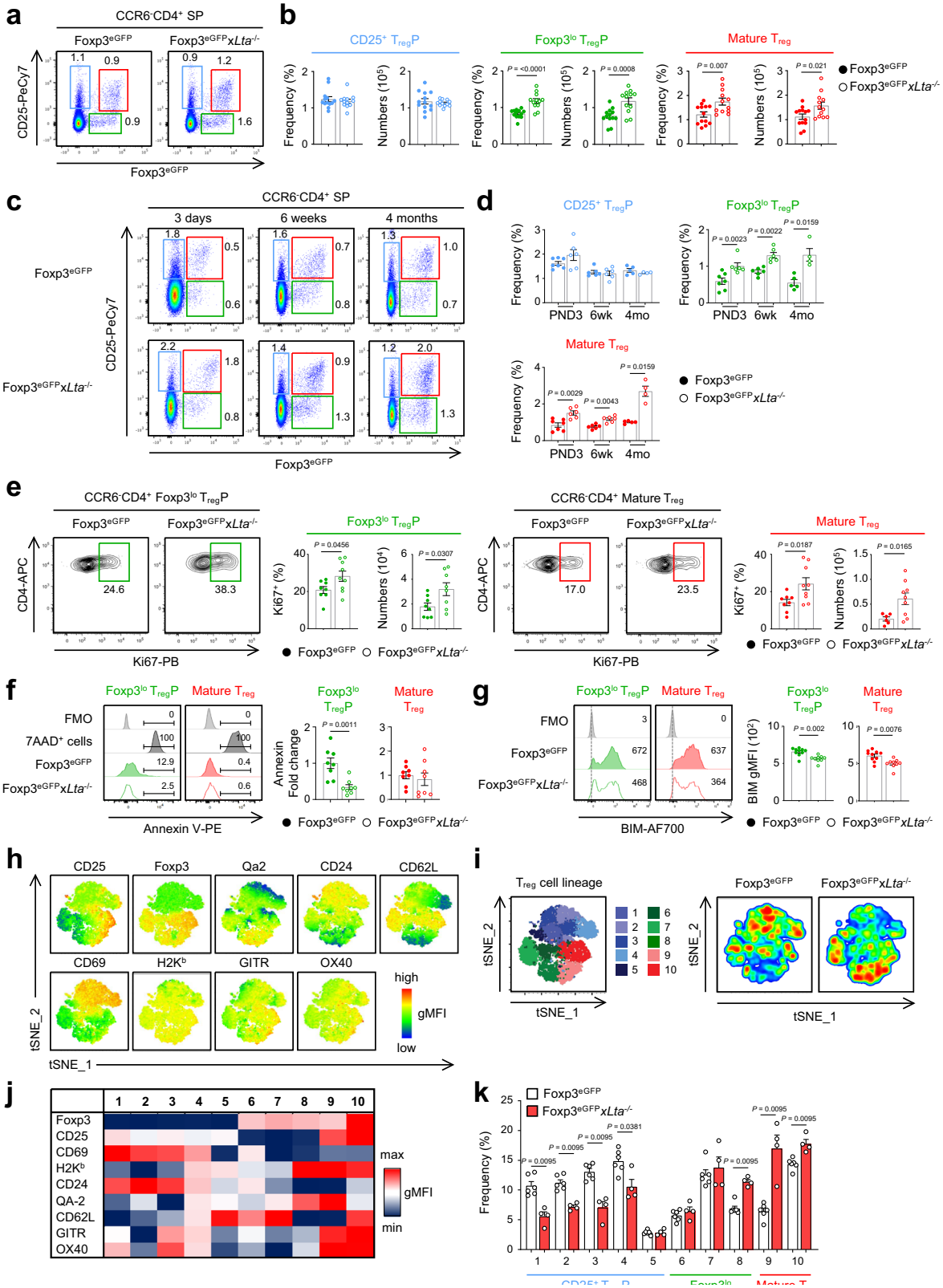

that CD25⁺ T_{reg}P subsets (clusters 2, 5 and 6) were underrepresented while clusters 7 and 8 corresponding to Foxp3^{lo} T_{reg}P and clusters 10 corresponding to mature T_{reg} were increased in Foxp3^{eGFP}x*Lta*$^{-/-}$ + WT → WT chimeras (Fig. 4f–h). Altogether, these data confirm that *Lta* expression in thymocytes negatively regulates the Foxp3^{lo} T_{reg}P developmental pathway, which could not be rescued by the reintroduction of WT cells.

Lta expression controls the metabolic profile of T_{reg} during their thymic development

To define the impact of *Lta* on T_{reg} development, we performed 3′-end single-cell RNA sequencing (scRNA-seq) on purified T_{reg} lineage cells from Foxp3^{eGFP} and Foxp3^{eGFP}x*Lta*$^{-/-}$ mice (Fig. 5a). Our analysis revealed that these cells separated into five distinct clusters (Fig. 5b, c). *Ccr7* expression was detected in all clusters, indicating that both T_{reg}P

Fig. 3 | *Lta* negatively regulates T_{reg} maturational development from Foxp3^{lo} T_{reg}P. a, **b** Representative flow cytometry profiles of CD25 and Foxp3 expression in CCR6$^-$CD4$^+$ SP thymocytes (**a**), frequencies and numbers (**b**) of CD25$^+$ T_{reg}P, Foxp3^{lo} T_{reg}P and mature T_{reg} from the thymus of Foxp3^{eGFP} (n = 13) and Foxp3^{eGFP}x*Lta*$^{-/-}$ (n = 12) mice. Data are pooled from four independent experiments. **c**, **d** Representative flow cytometry profiles, frequencies and numbers of CD25 and Foxp3 expression in CCR6$^-$CD4$^+$ SP thymocytes from 3 day- (n = 7 for Foxp3^{eGFP} and n = 6 for Foxp3^{eGFP}x*Lta*$^{-/-}$), 6 week- (n = 6 for Foxp3^{eGFP} and n = 6 for Foxp3^{eGFP}x*Lta*$^{-/-}$) and 4-month-(n = 5 for Foxp3^{eGFP} and n = 4 for Foxp3^{eGFP}x*Lta*$^{-/-}$) old mice. Data are pooled from 2 independent experiments. **e** Flow cytometry profiles, frequencies, and numbers of Ki67$^+$ cells in CCR6$^-$ Foxp3^{lo} T_{reg}P and mature T_{reg} of Foxp3^{eGFP} (n = 8) and Foxp3^{eGFP}x*Lta*$^{-/-}$ (n = 9) mice. Data are pooled from three independent experiments. **f** Representative annexin V staining and quantification in Foxp3^{lo} T_{reg}P and mature T_{reg} subsets from Foxp3^{eGFP} (n = 8) and Foxp3^{eGFP}x*Lta*$^{-/-}$ (n = 8) mice. 7AAD$^+$ dead cells were used as controls. The FMO is shown in T_{reg} subsets from Foxp3^{eGFP} mice. Data are pooled from two independent experiments. **(g)** BIM expression analyzed by flow cytometry in CCR6$^-$ Foxp3^{lo} T_{reg}P and mature T_{reg} subsets from Foxp3^{eGFP} (n = 10) and Foxp3^{eGFP}x*Lta*$^{-/-}$ (n = 9) mice. The FMO is shown in T_{reg} subsets from Foxp3^{eGFP} mice. Histograms show the quantification of BIM gMFI. Data are pooled from three independent experiments. **h**-**k** t-SNE dimensional reduction of flow cytometry data using maturation markers (**h**) allowing the identification of T_{reg} clusters in cells of the T_{reg} lineage identified in Supplementary Fig. 4a (**i**), fluorescence intensity heatmap of the markers used for the t-SNE construction of each T_{reg} cluster (**j**) and quantification of these clusters (**k**) in Foxp3^{eGFP} (n = 6) and Foxp3^{eGFP}x*Lta*$^{-/-}$ (n = 4) mice. Data are pooled from two independent experiments. Error bars show mean ± SEM, *p < 0.05, **p < 0.01, ***p < 0.001, and ****p < 0.0001 using unpaired two-tailed Student's t test for (**b**), (**e**–**f**) and unpaired two-tailed Mann–Whitney U test for (**d**), (**g**), (**k**). Source data are provided as a Source Data File.

and mature T_{reg} are located in the thymic medulla (Fig. 5d and Supplementary Fig. 6a). Clusters 0 and 1 exhibited an immature phenotype, characterized by the expression of *Cd24a* and *Cd69*, with no or poor *Foxp3*, *Sell* (CD62L) and *S1pr1* expression. While cluster 0 expressed *Il2rb* (CD122), *Il2rg* (CD132) and *Tnfrsf18* (GITR), cluster 1 also expressed *Il2ra* (CD25). This indicates that cluster 0 and 1 corresponded to T_{reg} pre-precursors (CD122$^+$CD25$^-$Foxp3$^-$)[31] and CD25$^+$ T_{reg}P, respectively. Cluster 2 expressed low levels of *Foxp3* and *Il2ra* in addition to high levels of TCR-signaling associated genes (*Nr4a1*, *Nr4a3*, and *Tnfrsf4*) (Fig. 5c, d), suggesting a transitional state towards mature T_{reg} (transitional T_{reg}). Cluster 3 expressed low levels of *Foxp3* while *Il2ra* was not detected, suggesting that cells from this cluster contained Foxp3^{lo} T_{reg}P. All cells from cluster 3 expressed *H2-K1* (H2K^b) while a fraction expressed *Cd69* (Fig. 5d and Supplementary Fig. 6a). In line with this observation, Foxp3^{lo} T_{reg}P contained mature CD69$^+$H2K^{b+} (M1) and CD69$^-$H2K^{b+} (M2) cells while CD25$^+$ T_{reg}P contained semi-mature CD69$^+$H2K^{b-} (SM), M1 and M2 cells (Supplementary Fig. 6b), indicating that Foxp3^{lo} T_{reg}P have a more mature phenotype than CD25$^+$ T_{reg}P. Accordingly, Foxp3^{lo} T_{reg}P resemble mature T_{reg} based on the differential expression of CD69 and H2K^b. Furthermore, we cannot exclude that cluster 3 included mature cells that could exit the thymus since high levels of *Sell*, *Klf2*, and *S1pr1* were detected. In line with this observation, we found that Foxp3^{lo} T_{reg}P expressed high level of CD62L by flow cytometry (Supplementary Fig. 6c). Cluster 4 expressed the highest levels of *Foxp3*, *Il2ra*, *Il2rb*, and *Il2rg*, suggesting that this cluster corresponded to CD25$^+$Foxp3$^+$ mature T_{reg} (Fig. 5d and Supplementary Fig. 6a), consistently with a high expression of *Sell*, *Klf2* and *S1pr1*.

We next performed trajectory analysis using the Monocle 3 package[32] to assess the developmental trajectory within the T_{reg} lineage. Three major branches were identified, starting at roots Y1, Y30, and Y2 all of which converged to Y16 located in cluster 4 corresponding to mature T_{reg}. (Supplementary Fig. 7a). The branch from Y1 to Y16 indicated a potential conversion of cells from cluster 0, to cluster 1, then to cluster 2, and finally to cluster 4. The Y30 to Y16 branch revealed another possible developmental route from cluster 0 directly to cluster 4. The branch from Y2 to Y16 indicated a short transition from cluster 3 to cluster 4. In line with the Seurat analysis (Fig. 5b–d), the progressive upregulation of *Foxp3* and *Il2ra* was associated with an upregulation of genes related to terminal maturation (*H2-K1*, *Sell* and *S1pr1*) along the pseudotime axis (Supplementary Fig. 7b).

We then compared changes in distinct cellular pathways in the different clusters of Foxp3^{eGFP} and Foxp3^{eGFP}x*Lta*$^{-/-}$ mice to analyze the impact of *Lta* on T_{reg} development (Fig. 5e). We calculated module scores of gene sets taken from the KEGG database and found metabolic pathways substantially altered by *Lta* deficiency. Although metabolic reprogramming regulates T_{reg} function in the periphery[33,34], the metabolic profile of thymic T_{reg} remains unknown. Our analysis revealed metabolic changes associated to T_{reg} development (Fig. 5f and Supplementary Fig. 7c). Interestingly, the module score for the oxidative phosphorylation (OXPHOS) gene set increased from cluster 0 (CD122$^+$CD25$^-$Foxp3$^-$ pre-T_{reg}P) to cluster 1 (CD25$^+$ T_{reg}P), then decreased in cluster 2 (Transitional T_{reg}) and further decreased in cluster 4 (Mature T_{reg}). We also found the module scores for glycolysis/gluconeogenesis, biosynthesis, and nucleotide metabolic pathways to be higher in cluster 1 compared to all other clusters, suggesting that CD25$^+$ T_{reg}P have a high metabolic activity. In line with these observations, cluster 1 highly expressed both OXPHOS (*Ndufa4*, *Ndufc2,* and *Atp5b*) and glycolysis (*Ldha*, *Pgk1,* and *Tpi1*) hallmark genes (Fig. 5g), while clusters 3 and 4 expressed mainly OXPHOS hallmark genes. On the other hand, there is likely no implication of the fatty acid metabolism during T_{reg} development suggested by the module score for this pathway (Fig. 5f). Compared to Foxp3^{eGFP} mice, clusters 2, 3 and 4 of Foxp3^{eGFP}x*Lta*$^{-/-}$ mice showed an enhanced score for OXPHOS metabolism, indicating that *Lta* expression regulates the metabolic profile of the most mature T_{reg} subsets (Fig. 5f and Supplementary Fig. 7d).

Given that scRNA-seq data suggest gene expression changes of OXPHOS-related genes during T_{reg} development (Fig. 5f), we then analyzed mitochondrial activity. In line with the transcriptomic analysis, CD25$^+$ T_{reg}P displayed higher mitochondrial activity compared to Foxp3^{lo} T_{reg}P and mature T_{reg}, as shown by MitoTracker Deep Red staining (Fig. 6a). CD25$^+$ T_{reg}P and Foxp3^{lo} T_{reg}P of Foxp3^{eGFP}x*Lta*$^{-/-}$ mice showed fewer active mitochondria compared to their respective control counterparts (Fig. 6b). Since this functional defect in mitochondrial polarization was unforeseen in scRNA-seq data, we further analyzed the metabolic profile of developing T_{reg} using a functional assay. Given that low numbers of T_{reg}P can be retrieved from the thymus, we took advantage of the newly developed flow-cytometry-based method, SCENITH™ (Single-Cell Metabolism by Profiling Translation Inhibition)[35], to analyze the metabolic profiles of T_{reg}P and mature T_{reg}. This method is based on metabolism-dependent translation rates and puromycin incorporation into nascent proteins in response to specific metabolic inhibitors. Thus, SCENITH™ permits the assessment of glucose dependency, mitochondrial dependency, glycolytic capacity as well as fatty acid and amino acid oxidation capacity in multiple rare cell types simultaneously. In line with our transcriptomic (Fig. 5f) and MitoTracker analysis (Fig. 6a), CD25$^+$ T_{reg}P showed higher levels of protein synthesis than Foxp3^{lo} T_{reg}P and mature T_{reg} (Supplementary Fig. 8a), further confirming that CD25$^+$ T_{reg}P are more metabolically active. Strikingly, CD25$^+$ T_{reg}P and Foxp3^{lo} T_{reg}P showed a distinct metabolic profile (Fig. 6c and Supplementary Fig. 8b), with Foxp3^{lo} T_{reg}P being more similar to mature T_{reg}. Specifically, CD25$^+$ T_{reg}P showed 50% dependency on both glucose and mitochondrial OXPHOS, while Foxp3^{lo} T_{reg}P showed 85% mitochondrial dependency similar to the 75% mitochondrial dependency of mature T_{reg} (Fig. 6c). These results are in accordance with the OXPHOS

https://doi.org/10.1038/s41467-024-51164-5

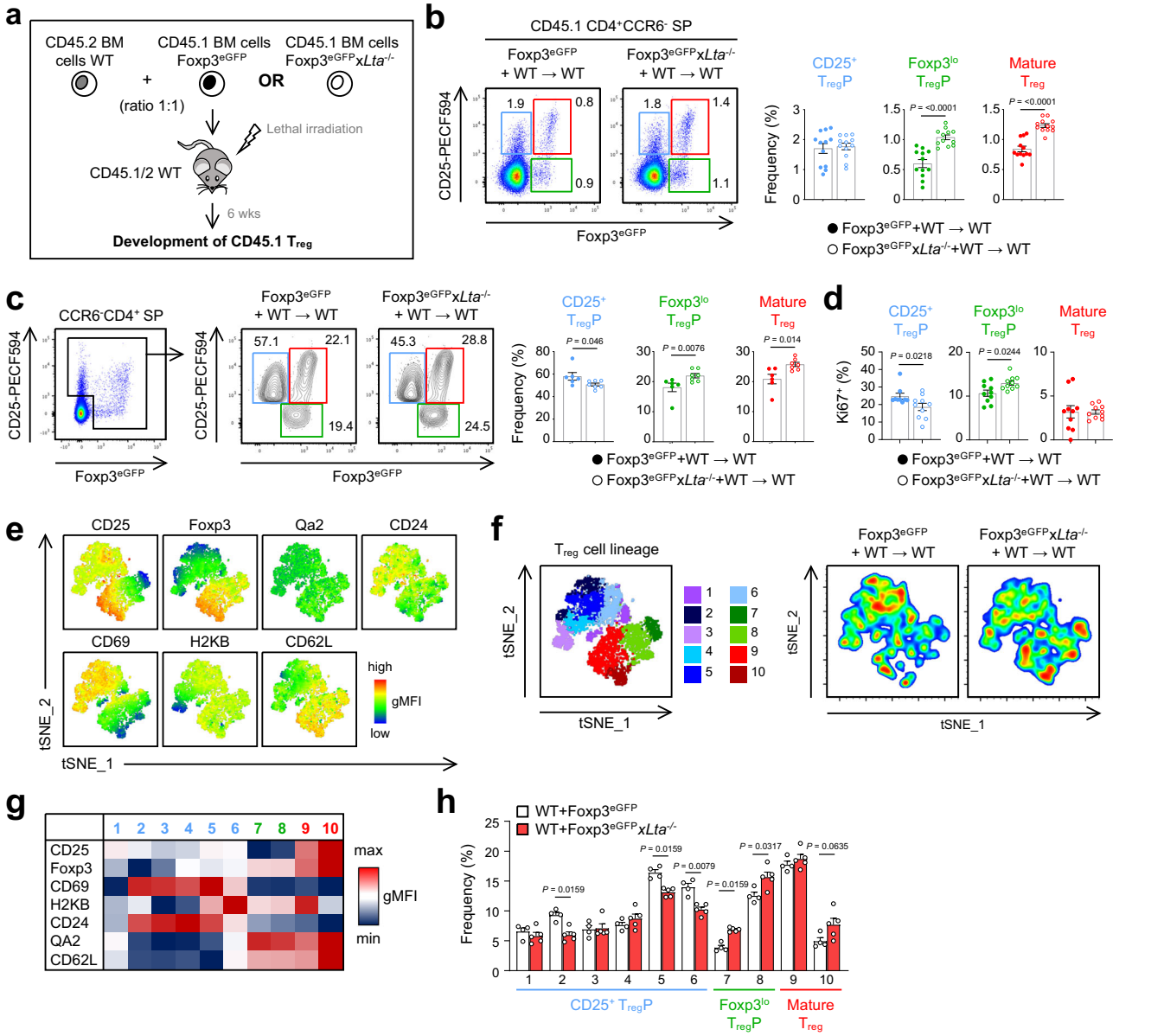

Fig. 4 | Hematopoietic origin of *Lta* expression regulates thymic T_{reg} development. a Experimental set up: lethally irradiated CD45.1/2 WT recipients were reconstituted with CD45.2 WT + CD45.1 Foxp3^{eGFP} or Foxp3^{eGFP}x*Lta*$^{-/-}$ (ratio 1:1) mixed BM cells. Six weeks later, CD45.1 CCR6$^-$ T_{reg} were analyzed in the thymus of recipient mice. **b** Flow cytometry profiles and frequencies of CD25$^+$ T_{reg}P, Foxp3^{lo} T_{reg}P and mature T_{reg} from CD45.1 Foxp3^{eGFP} (n = 12) or Foxp3^{eGFP}x*Lta*$^{-/-}$ (n = 12) BM cells. Data are pooled from four independent experiments. **c** Representative flow cytometry profiles and frequencies of CD25$^+$ T_{reg}P, Foxp3^{lo} T_{reg}P, and mature T_{reg} in the T_{reg} cell lineage gate derived from CD45.1 Foxp3^{eGFP} (n = 6) or Foxp3^{eGFP}x*Lta*$^{-/-}$ (n = 7) BM cells. Data are pooled from two independent experiments. **d** Frequencies of Ki67$^+$ cells in CD25$^+$ T_{reg}P (n = 9 for Foxp3^{eGFP} and n = 10 for Foxp3^{eGFP}x*Lta*$^{-/-}$), Foxp3^{lo} T_{reg}P (n = 10) and mature T_{reg} (n = 10) derived from CD45.1 Foxp3^{eGFP} or Foxp3^{eGFP}x*Lta*$^{-/-}$ BM cells. Data are pooled from three independent experiments. **e**-**h** t-SNE dimensional reduction of flow cytometry data using maturation markers (**e**) allowing the identification of T_{reg} clusters (**f**), fluorescence intensity heatmap of the markers used for the t-SNE construction of each T_{reg} cluster (**g**), and quantification of these clusters (**h**) in cells derived from CD45.1 Foxp3^{eGFP} (n = 4) or Foxp3^{eGFP}x*Lta*$^{-/-}$ (n = 5) BM cells. Data are pooled from two independent experiments. Error bars show mean ± SEM, *p < 0.05, **p < 0.01, and ****p < 0.0001 using unpaired two-tailed Student's t test for (**b**) and unpaired two-tailed Mann–Whitney U test for (**c**), (**d**) and (**h**). Source data are provided as a Source Data File.

and glycolysis/gluconeogenesis module scores calculated using our scRNA-seq analysis at steady state (Fig. 5f). Interestingly, we found that Foxp3^{lo} T_{reg}P and mature T_{reg} from Foxp3^{eGFP}x*Lta*$^{-/-}$ mice exhibited an exacerbated glucose dependency (Fig. 6d and Supplementary Fig. 8c, d).

Next, we further explored the metabolic profiles of the distinct maturational stages of T_{reg}P and mature T_{reg} cells using CD69 and H2K^b developmental markers (Fig. 6e)[36]. In wild-type conditions, the mitochondrial dependence increased while the glycolytic capacity decreased during CD25$^+$ T_{reg}P maturation (Fig. 6f). We further found a distinct metabolic profile for the M1 subset within CD25$^+$ and Foxp3^{lo} T_{reg}P, whereby M1 Foxp3^{lo} T_{reg}P exhibited a higher mitochondrial dependence. Notably, CD25$^+$ and Foxp3^{lo} T_{reg}P M2 subsets had a similar metabolic profile compared to M1 and M2 mature T_{reg} whose profile was characterized by a high mitochondrial dependency and a low glycolytic capacity. A similar profile was also observed in the Foxp3^{lo} T_{reg}P M1 subset. These results suggest that the increase in mitochondrial dependency is tightly linked to T_{reg} maturation. In Foxp3^{eGFP}x*Lta*$^{-/-}$ mice, CD25$^+$ T_{reg}P SM cells showed an increased

https://doi.org/10.1038/s41467-024-51164-5

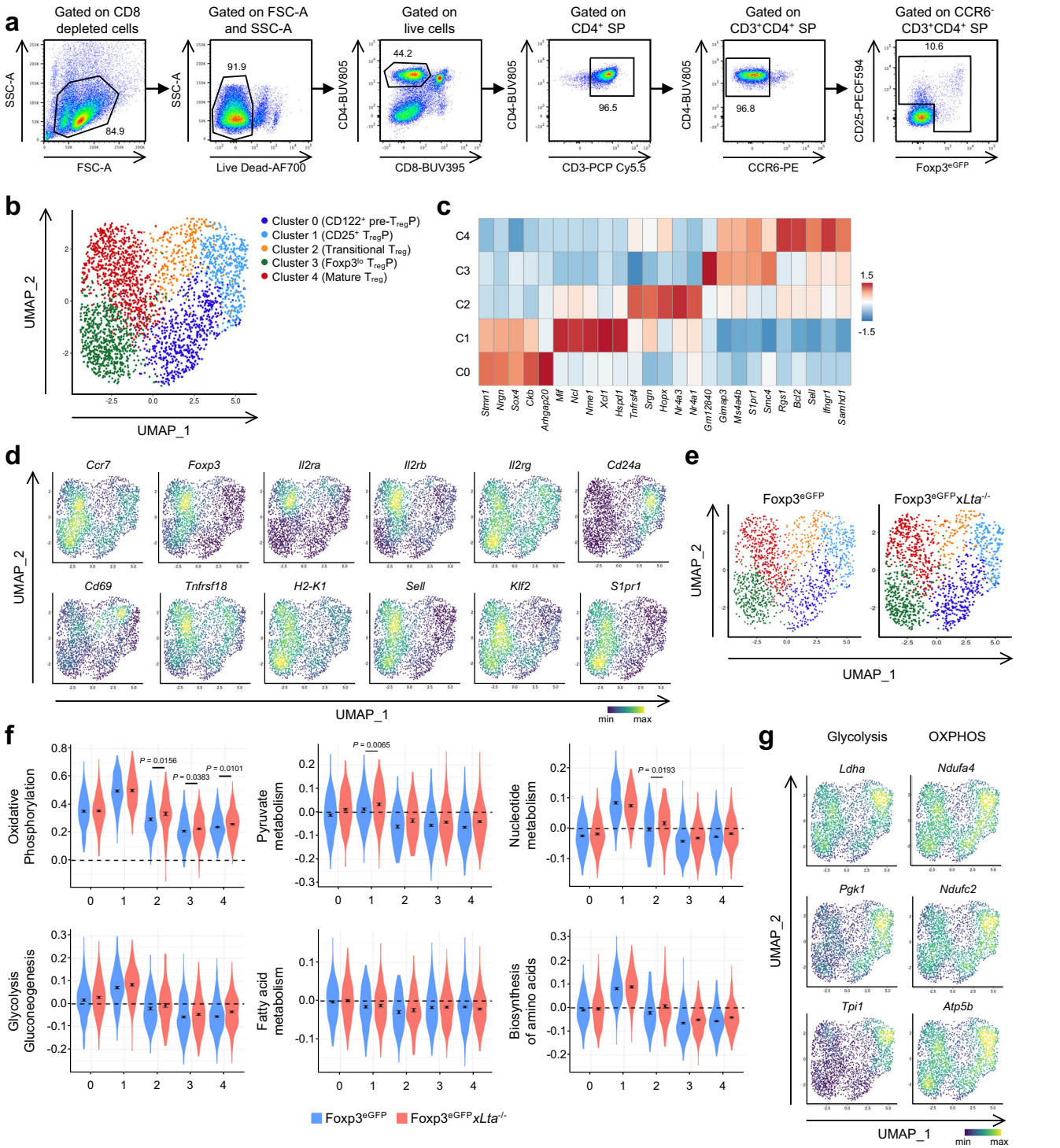

Fig. 5 | Single-cell RNA sequencing reveals that *Lta* deficiency affects the metabolic program of developing T_{reg} subsets. a Gating strategy used to purify T_{reg} lineage cells from Foxp3^{eGFP} and Foxp3^{eGFP}x*Lta*$^{-/-}$ mice. **b** Merged UMAP visualization of T_{reg} lineage cells colored by cell types from Foxp3^{eGFP} and Foxp3^{eGFP}x*Lta*$^{-/-}$ mice. **c** Heatmap showing the expression level of the top 5 differentially expressed genes (adj-p-val<0.001) in each cluster. **d** Density scores of T_{reg} markers, *Foxp3*, *Il2ra*, *Il2rb* and *Il2rg*, as well as maturation markers, *Ccr7*, *Cd24a*, *Cd69*, *Tnfrsf18*, *H2-K1*, *Sell*, *Klf2* and *S1pr1* on merged data from Foxp3^{eGFP} and Foxp3^{eGFP}x*Lta*$^{-/-}$ mice. Scores were computed using the Nebulosa package in R. **e** UMAP visualization of T_{reg} lineage cells from Foxp3^{eGFP} (1433 cells) and Foxp3^{eGFP}x*Lta*$^{-/-}$ (1342 cells) mice. **f** Module score distributions per condition and cluster for various metabolic pathways. **g** Density scores of glycolysis-associated genes (*Ldha*, *Pgk1*, and *Tpi1*) and OXPHOS-associated genes (*Ndufa4*, *Ndufc2*, and *Atp5b*) on merged data from Foxp3^{eGFP} and Foxp3^{eGFP}x*Lta*$^{-/-}$ mice. Scores were computed using the Nebulosa package in R. Statistical comparison of module scores between conditions for each cluster was performed using the Wilcoxon test with Benjamini-Hochberg multitest correction. Error bars show mean ± SD, *p < 0.05, **p < 0.01. Source data are provided as a Source Data File.

https://doi.org/10.1038/s41467-024-51164-5

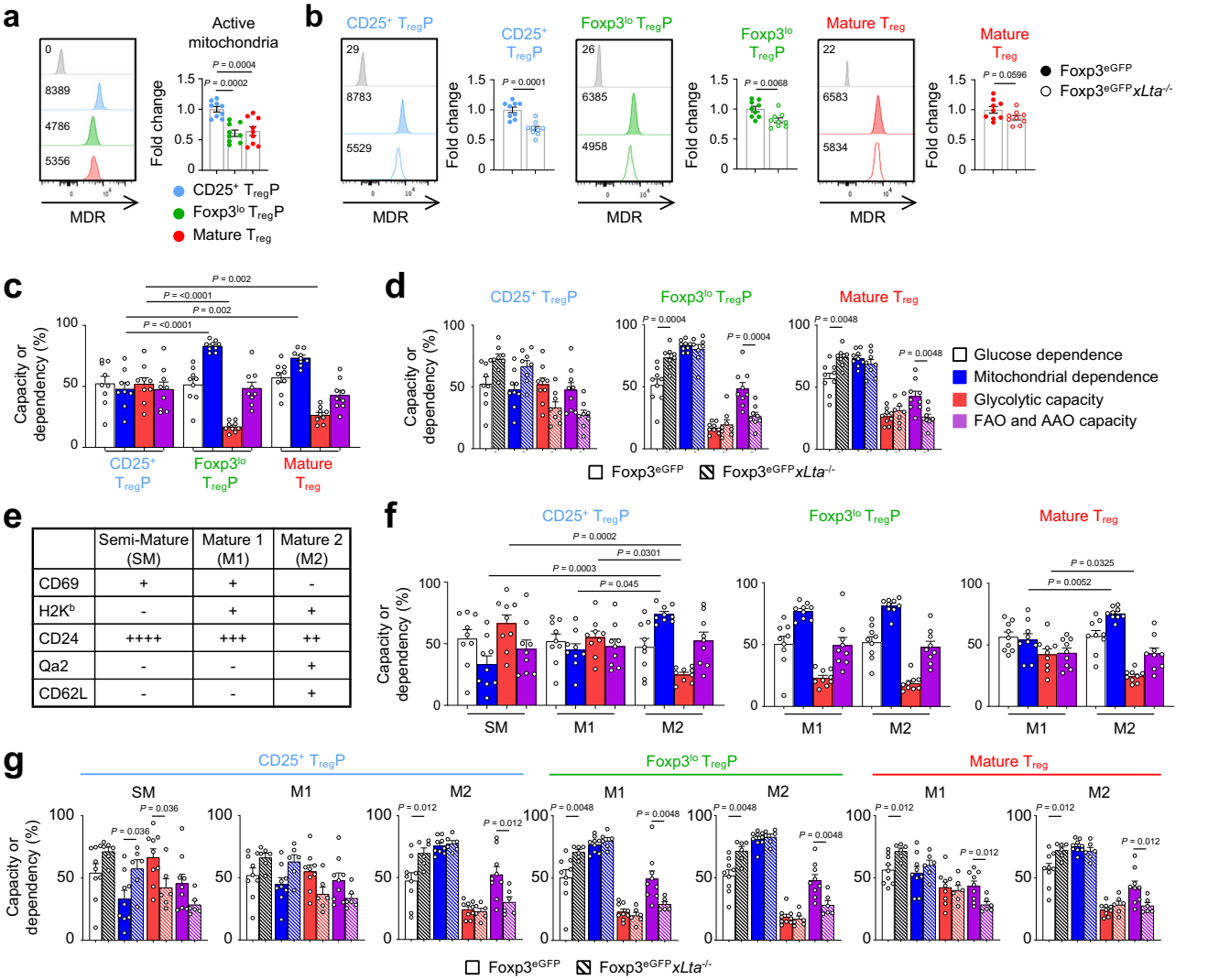

	Semi-Mature (SM)	Mature 1 (M1)	Mature 2 (M2)
CD69	+	+	-
H2K^b	-	+	+
CD24	++++	+++	++
Qa2	-	-	+
CD62L	-	-	+

Fig. 6 | LTα$_1$β$_2$ expression regulates T$_{reg}$ glucose dependence during their development. a, **b** Representative histogram and fold change in the gMFI of MitoTracker Deep Red (MDR) staining in CCR6$^-$ CD25$^+$ T$_{reg}$P, Foxp3^{lo} T$_{reg}$P and mature T$_{reg}$ from Foxp3^{eGFP} (n = 9) mice (**a**) compared to Foxp3^{eGFP}x*Lta*$^{-/-}$ (n = 9) mice (**b**). FMO are shown in Foxp3^{eGFP} T$_{reg}$ subsets. Data are pooled from two independent experiments. **c**, **d** SCENITH metabolic profiling of CD25$^+$ T$_{reg}$P, Foxp3^{lo} T$_{reg}$P, and mature T$_{reg}$ from Foxp3^{eGFP} (n = 9) (**c**) and Foxp3^{eGFP}x*Lta*$^{-/-}$ (n = 8) (**d**) mice. Graphs show the percentage of glucose dependence, mitochondrial dependence, glycolytic capacity as well as fatty acid and amino acid (FAO and AAO) capacity of each cell subset. Data are pooled from three independent experiments. **e** The table summarizes the phenotype of semi-mature (SM), mature 1 (M1) and mature 2 (M2) CD4$^+$ SP thymocytes. **f**, **g** SCENITH metabolic profiling depending on maturational state of CD25$^+$ T$_{reg}$P, Foxp3^{lo} T$_{reg}$P, and mature T$_{reg}$ from Foxp3^{eGFP} (n = 9) and Foxp3^{eGFP}x*Lta*$^{-/-}$ (n = 6) mice. Data are pooled from three independent experiments. Error bars show mean ± SEM, *p < 0.05, **p < 0.01, ***p < 0.001, and ****p < 0.0001 using one-way ANOVA for (**a**), (**c**) and (**f**), unpaired two-tailed Student's t test for (**b**) and (**d**), unpaired two-tailed Mann–Whitney U test for (**g**). Source data are provided as a Source Data File.

mitochondrial dependence while the M2 cells exhibited an increased glucose dependence (Fig. 6g). Moreover, the glucose dependence was also increased in Foxp3^{lo} T$_{reg}$P and mature T$_{reg}$ at M1 and M2 stages. Thus, Foxp3^{lo} T$_{reg}$P display a similar metabolic profile to the most mature T$_{reg}$ (M2) and *Lta* expression negatively regulates their glucose dependency. Overall, these findings show that LTα modulates the metabolic profile of T$_{reg}$ along their maturational development.

LTα$_1$β$_2$-regulated T$_{reg}$ development depends on IL-4 production by mTEC

We then investigated the underlying mechanism of LTα$_1$β$_2$-LTβR-regulated T$_{reg}$ development. We made the hypothesis that the LTα$_1$β$_2$-LTβR axis could regulate the expression of cytokines. Consistent with a previous report[15], we found that *Il4ra* was preferentially expressed in Foxp3^{lo} T$_{reg}$P compared to CD25$^+$ T$_{reg}$P, and its expression was further upregulated in mature T$_{reg}$ at both mRNA and protein levels (Fig. 7a, b). In contrast, cells of the T$_{reg}$ lineage did not produce IL-4, ruling out an autocrine stimulation (Fig. 7a). This expression pattern suggests that IL-4 may support the conversion of Foxp3^{lo} T$_{reg}$P into CD25$^+$Foxp3$^+$ mature T$_{reg}$. To test this hypothesis, purified CD25$^+$ T$_{reg}$P and Foxp3^{lo} T$_{reg}$P were stimulated with increasing doses of IL-4. In contrast to CD25$^+$ T$_{reg}$P, IL-4 stimulation promoted the robust conversion of Foxp3^{lo} T$_{reg}$P into CD25$^+$Foxp3$^+$ mature T$_{reg}$ (Fig. 7c and Supplementary Fig. 9). Interestingly, we found increased *Il4* expression in the thymus of *Lta*$^{-/-}$ mice, which was associated with enhanced development of IL-4-dependent Eomes$^+$ memory-like CD8$^+$ SP thymocytes[37,38] (Fig. 7d, e). Furthermore, frequencies and numbers of phospho-Stat6$^+$ cells were substantially enhanced, further highlighting an IL-4-rich environment in the thymus of *Lta*$^{-/-}$ mice (Supplementary Fig. 10a). Among these cells, frequencies of phospho-Stat6$^+$ mature T$_{reg}$ were increased in *Lta*$^{-/-}$ mice (Supplementary Fig. 10b), suggesting that

https://doi.org/10.1038/s41467-024-51164-5

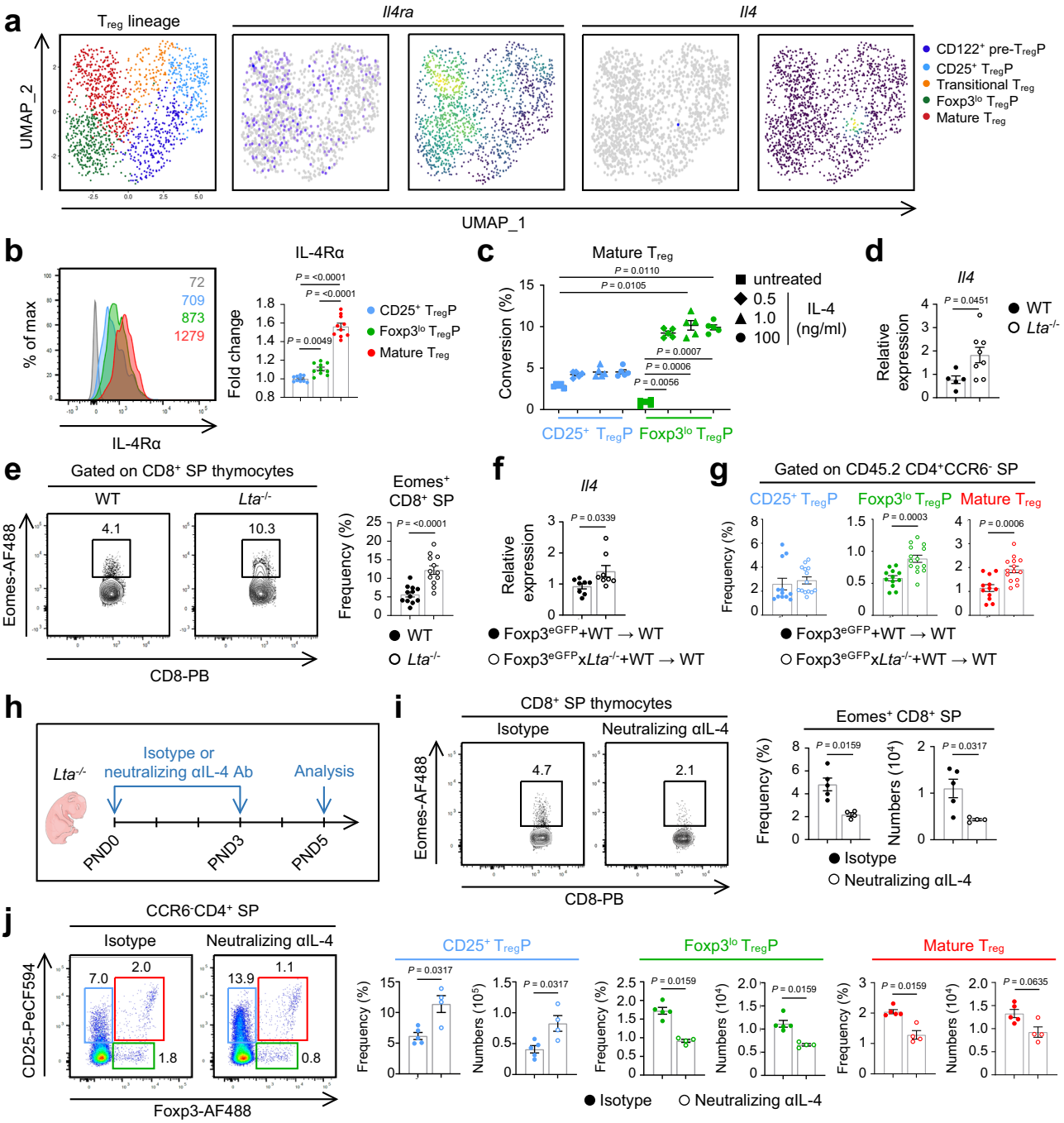

Fig. 7 | IL-4 controls the Foxp3^{lo} T$_{reg}$P developmental pathway in the thymus. **a** UMAP visualization of T$_{reg}$ lineage cells colored by cell types (left), feature, and density UMAP representation of *Il4ra* (middle) *and Il4* (right) expression from Foxp3^{eGFP} mice. **b** Representative histogram and fold change in the gMFI of IL-4Rα in CD25$^+$ T$_{reg}$P, Foxp3^{lo} T$_{reg}$P, and mature T$_{reg}$ identified in CCR6$^-$CD4$^+$ SP thymocytes from Foxp3^{eGFP} mice (n = 10). The FMO is shown in the CD25$^+$Foxp3^{eGFP} T$_{reg}$ subset. Data are pooled from three independent experiments. **c** Frequencies of CD25$^+$Foxp3$^+$ mature T$_{reg}$ generated from purified CD25$^+$ T$_{reg}$P or Foxp3^{lo} T$_{reg}$P stimulated with 0.5 ng/mL (diamond, n = 5), 1.0 ng/mL (triangle, n = 5), 100 ng/mL of IL-4 (circle, n = 5) or unstimulated (square, n = 5). Data are pooled from two independent experiments. **d** Relative expression of *Il4* in the thymus of WT (n = 5) and *Lta*$^{-/-}$ (n = 8) mice. Data are pooled from two independent experiments. **e** Flow cytometry profiles and frequencies of Eomes$^+$ CD8$^+$ SP thymocytes from WT (n = 12) or *Lta*$^{-/-}$ (n = 12) mice. Data are pooled from two independent experiments. **f** Relative expression of *Il4* in the thymus of mixed BM chimeras (Foxp3^{eGFP}+WT mice, n = 8 and Foxp3^{eGFP}x*Lta*$^{-/-}$+WT mice, n = 8). Data are pooled from two independent experiments. **g** Frequencies of CCR6$^-$ CD25$^+$ T$_{reg}$P, Foxp3^{lo} T$_{reg}$P, and mature T$_{reg}$ derived from CD45.2 BM cells (Foxp3^{eGFP}+WT mice; n = 12 and Foxp3^{eGFP}x*Lta*$^{-/-}$+WT mice; n = 14). Data are pooled from three independent experiments. **h** Experimental set-up: *Lta*$^{-/-}$ mice were injected i.p. with neutralizing anti-IL4 antibody or isotype control at postnatal day (PND) 0 and PND3. Pups were sacrificed at PND5. **i, j** Representative flow cytometry profiles, frequencies, and numbers of Eomes$^+$ CD8$^+$ SP thymocytes (**i**) and CCR6$^-$CD4$^+$ CD25$^+$ T$_{reg}$P, Foxp3^{lo} T$_{reg}$P, and mature T$_{reg}$ (**j**) from the thymus of *Lta*$^{-/-}$ pups injected with an isotype control (n = 5) or a neutralizing anti-IL4 antibody (n = 4). Data are pooled from two independent experiments. Error bars show mean ± SEM, *p < 0.05, **p < 0.01, ***p < 0.001 and ****p < 0.0001 using one-way ANOVA for (**b**), Kruskal–Wallis test for (**c**), unpaired two-tailed Mann–Whitney U test for (**d**) and (**i**, **j**) and unpaired two-tailed Student's t test for (**e**–**g**). Source data are provided as a Source Data File.

https://doi.org/10.1038/s41467-024-51164-5

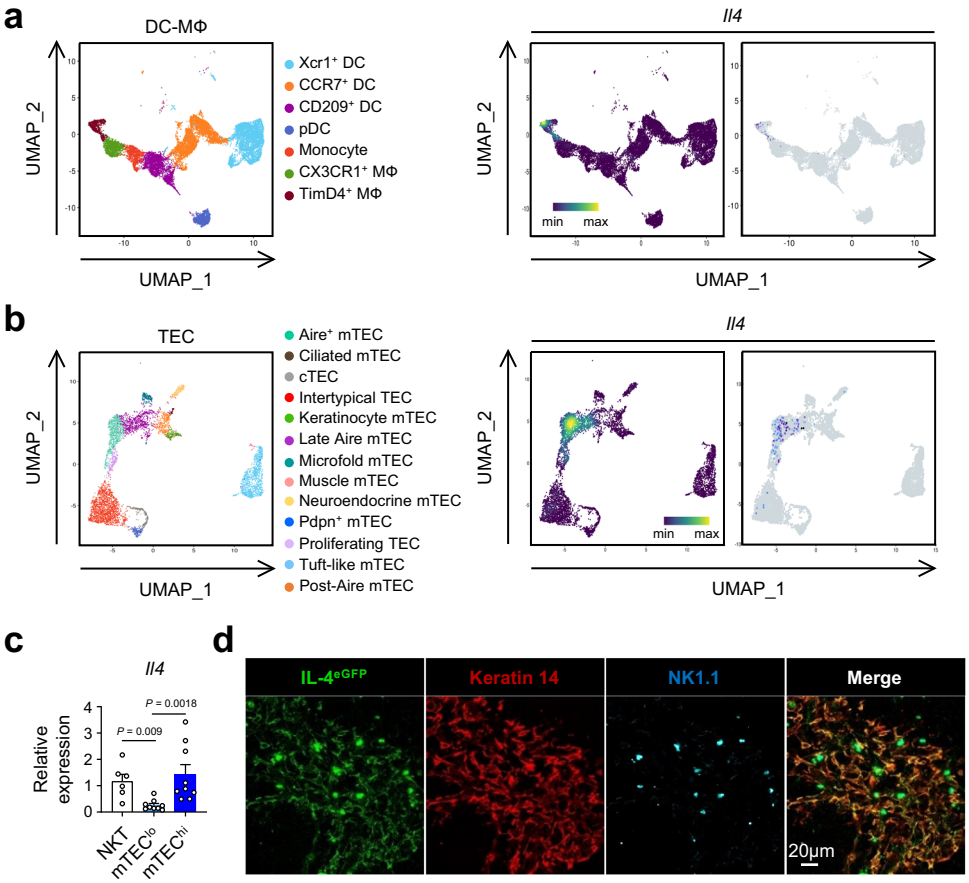

Fig. 8 | mTEC are a novel source of IL-4 in the thymus. a UMAP visualization of DC and macrophage subsets colored by cell types (left). Density and feature UMAP representation of *Il4* expression in DC and macrophage subsets (right). **b** UMAP visualization of TEC subsets colored by cell types (left). *Il4* expression projected on UMAP visualization of TEC subsets (right). **c** Relative expression of *Il4* in thymic NKT (n = 6), mTEC^{lo} (n = 9), and mTEC^{hi} (n = 9) from WT mice. Data are pooled from two independent experiments. **d** Confocal images of the thymus of 4get C57BL/6 mice showing IL-4^{eGFP} (green), keratin 14 (red), and NK1.1 (blue) staining. Scale bar, 20 μm. Image representative of 3 mice. Error bars show mean ± SEM, **p < 0.01 using Kruskal–Wallis test for (**c**). Source data are provided as a Source Data File.

enhanced IL-4 expression affects mature T_{reg}. In line with enhanced Foxp3^{lo} T_{reg}P and mature T_{reg} in Foxp3^{eGFP}x*Lta*$^{-/-}$ + WT → WT chimeras (Fig. 4), *Il4* expression was higher in the thymus of those recipients, which was associated with increased frequencies of phospho-Stat6^{+} thymocytes (Fig. 7f and Supplementary Fig. 10c). Moreover, in line with the reintroduction of WT BM cells in these chimeras, IL-4 and phospho-Stat6 levels increased by only half of those observed in *Lta*$^{-/-}$ mice. This partial increase in *Il4* expression was sufficient to enhance the frequencies of Foxp3^{lo} T_{reg}P and mature T_{reg} of CD45.2 WT origin (Fig. 7g). This indicates that the Foxp3^{lo} T_{reg}P developmental pathway is highly sensitive to subtle variations in IL-4 levels. To investigate the role of IL-4 in vivo in T_{reg} development, *Lta*$^{-/-}$ pups were injected with an anti-IL-4 neutralizing antibody during the emergence of T_{reg}P at post-natal day 0 and 3 (Fig. 7h). Five days after birth, Eomes^{+} memory-like CD8^{+} SP thymocytes were reduced, showing the effectiveness of IL-4 neutralization (Fig. 7i). Interestingly, frequencies and numbers of Foxp3^{lo} T_{reg}P and CD25^{+}Foxp3^{+} mature subsets were substantially reduced while CD25^{+} T_{reg}P were over-represented (Fig. 7j). These results suggest that IL-4 favors the Foxp3^{lo} T_{reg}P developmental pathway at the expense of the CD25^{+} T_{reg}P pathway.

Although type 2 natural killer T cells (NKT2) are an important source of IL-4 in the thymus[37–39], increased expression of *Il4* in *Lta*$^{-/-}$ mice was unlikely due to NKT2 cell enrichment (Supplementary Fig. 10d), suggesting another cellular source of IL-4. We therefore explored whether other thymic cells may express *Il4*. Using a scRNA-seq dataset[40], we found that *Il4* was not expressed by thymic DC and macrophages (Fig. 8a). We next investigated the possibility that mTEC could produce this cytokine and found that IL-4 was mainly expressed by Aire^{+} mTEC^{hi} and late-Aire mTEC in scRNA-seq datasets (Fig. 8b). We confirmed by qPCR that the level of *Il4* was higher in mTEC expressing high levels of the CD80 costimulatory molecule (mTEC^{hi}) than in mTEC expressing low levels of CD80 (mTEC^{lo}) and that the level in mTEC^{hi} was similar to that observed in NKT cells (Fig. 8c). Using IL-4 reporter mice on a C57BL/6 or BALB/c background, IL-4 expression was detected both in NKT cells and mTEC (Fig. 8d and Supplementary Fig. 10e), confirming that mTEC constitute a substantial source of IL-4 in the thymus. Given that the classical NF-κB member p65 (RelA) was reported to upregulate *Il4* expression by binding to its promoter[41], we assessed its expression in mTEC^{hi} of *Lta*$^{-/-}$ mice and found enhanced protein levels of p65 (Supplementary Fig. 10f). This suggests that the increased expression of p65 may lead to elevated *Il4* expression in mTEC^{hi} of *Lta*$^{-/-}$ mice.

Given that mTEC control the generation of CD25^{+}Foxp3^{+} T_{reg}[2,3,42–44], we explored the expression of LTβR within mTEC subsets by reanalysing TEC scRNA-seq datasets[45,46]. *Ltbr* was widely expressed in mTEC subsets (Supplementary Fig. 11a). We confirmed by flow cytometry this wide expression in mTEC^{lo} and mTEC^{hi} (Supplementary Fig. 11b,c). Next, we analyzed the TEC scRNA-seq with our thymic T_{reg} scRNA-seq datasets to identify possible cell-cell interactions via the $LT\alpha_1\beta_2$-LTβR axis using CellChat[47]. CD25^{+} T_{reg}P and Foxp3^{lo} T_{reg}P likely interact with several mTEC subsets (Supplementary Fig. 11d). These interactions seemed to be stronger with transitional and mature T_{reg},

https://doi.org/10.1038/s41467-024-51164-5

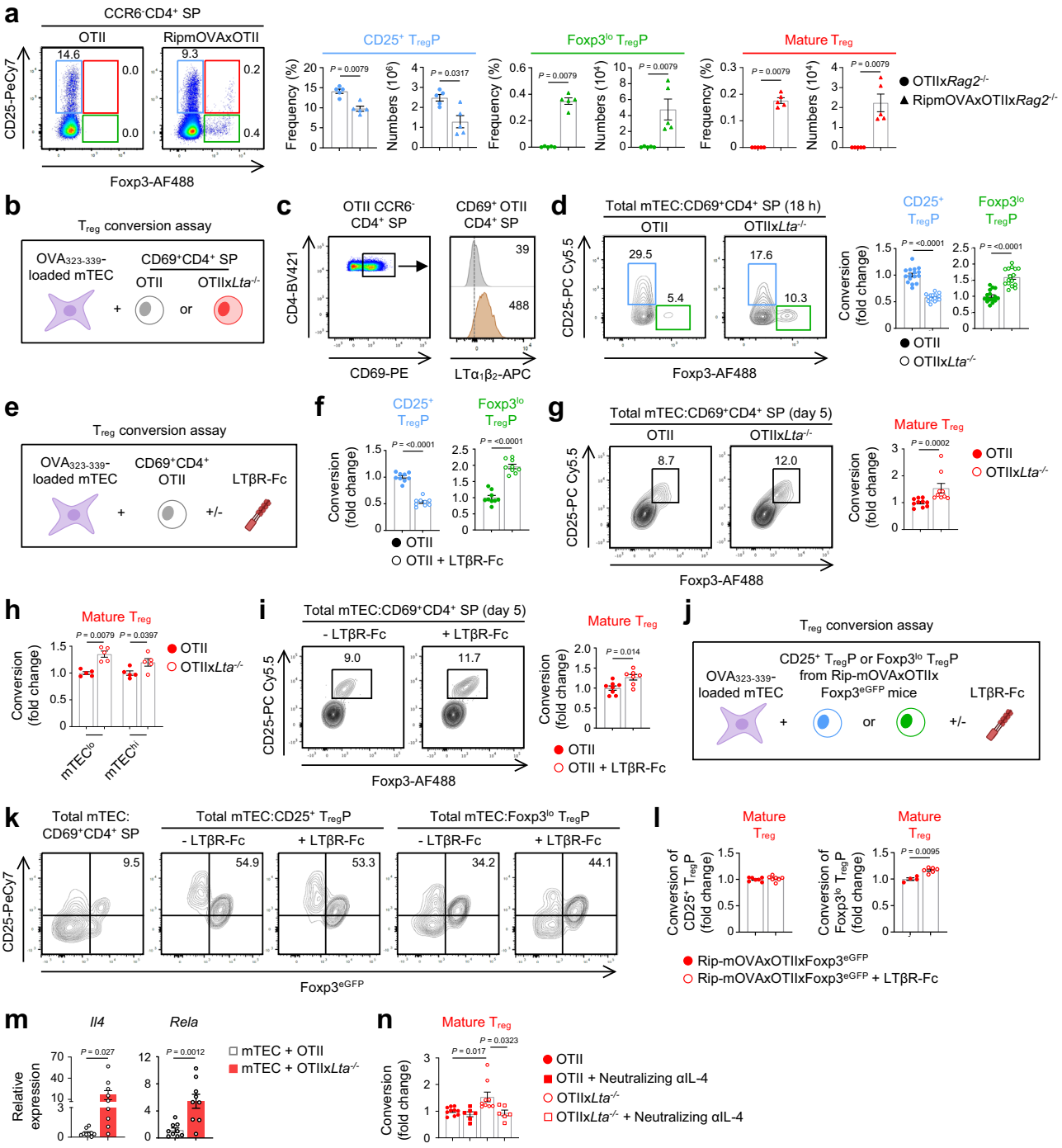

consistent with the gradual increase of $LT\alpha_1\beta_2$ expression during T_{reg} development (Fig. 1c and Supplementary Fig. 1c).

Next, to determine the contribution of mTEC in $LT\alpha_1\beta_2$-LTβR-regulated T_{reg} development, we used OTII transgenic mice that possess $CD4^+$ SP thymocytes expressing an MHCII-restricted TCR specific for the chicken ovalbumin (OVA). First, we verified that OTII cells transit through the $CD25^+$ and $Foxp3^{lo}$ $T_{reg}P$ developmental pathways. To this end, we took advantage of RipmOVAxOTIIx*Rag2*$^{-/-}$ mice in which the Rat Insulin Promoter (Rip) drives the expression of the membrane-bound OVA (mOVA) form specifically in mTEC. In these transgenic mice, high-affinity interactions between OVA-expressing mTEC and OTII thymocytes are possible in vivo. Whereas $Foxp3^{lo}$ $T_{reg}P$ and $CD25^+Foxp3^+$ mature T_{reg} were undetectable in OTIIx*Rag2*$^{-/-}$ mice, these two T_{reg} subsets developed in RipmOVAxOTIIx*Rag2*$^{-/-}$ mice, indicating that OTII thymocytes transit through $Foxp3^{lo}$ $T_{reg}P$ toward mature T_{reg} when the cognate self-antigen is expressed in mTEC (Fig. 9a). We then performed in vitro antigen-specific T_{reg} conversion assays in which WT mTEC loaded with the $OVA_{323-339}$ peptide were co-cultured with $CD69^+$ semi-mature OTII $CD4^+$ SP thymocytes, that expressed the membrane-bound $LT\alpha_1\beta_2$ and were shown to contain cells with a high ability to differentiate into mature T_{reg}[42] (Fig. 9b, c). After 18 h of co-culture, mTEC presenting the cognate antigen had the capacity to induce $Foxp3^{lo}$ $T_{reg}P$, further confirming that OTII thymocytes transit via a $Foxp3^{lo}$ $T_{reg}P$ stage (Fig. 9d). To further investigate the role of *Lta*, we performed this experiment with $CD69^+CD4^+$ SP thymocytes purified from OTII mice backcrossed on an *Lta*$^{-/-}$ background (OTIIx*Lta*$^{-/-}$ mice). Interestingly, the conversion in $Foxp3^{lo}$ $T_{reg}P$ increased while

Fig. 9 | The LTα$_1$β$_2$-LTβR axis provided by mTEC limits Foxp3^{lo} T$_{reg}$ development in an IL-4 dependent manner. a Representative flow cytometry profiles, frequencies, and numbers of thymic CCR6$^-$CD4$^+$ CD25$^+$ T$_{reg}$P, Foxp3^{lo} T$_{reg}$P and mature T$_{reg}$ from OTIIx*Rag2*$^{-/-}$ and RipmOVAxOTIIx*Rag2*$^{-/-}$ mice (n = 5 from two independent experiments). **b** T$_{reg}$ conversion assay: OVA$_{323-339}$-loaded mTEC were co-cultured with CD69$^+$ semi-mature CD4$^+$ thymocytes from OTII or OTIIx*Lta*$^{-/-}$ mice. **c** LTα$_1$β$_2$ expression in CD69$^+$ OTII CD4$^+$ thymocytes compared to control (II ab). **d** Flow cytometry profiles and fold change in the frequencies of CD25$^+$ and Foxp3^{lo} T$_{reg}$P derived from CD69$^+$ OTII or OTIIx*Lta*$^{-/-}$ CD4$^+$ thymocytes after 18 h of co-culture (n = 16 from two independent experiments). **e** T$_{reg}$ conversion assay: OVA$_{323-339}$-loaded mTEC were co-cultured with CD69$^+$ semi-mature CD4$^+$ thymocytes pretreated or not with the blocking LTβR-Fc receptor. **f** Flow cytometry profiles and fold change in the frequencies of CD25$^+$ and Foxp3^{lo} T$_{reg}$P derived from CD69$^+$ OTII CD4$^+$ thymocytes pretreated or not with the blocking LTβR-Fc receptor after 18 h of co-culture (n = 9 from two independent experiments). **g**, **h** Flow cytometry profiles and fold change in the frequencies of CD25$^+$Foxp3$^+$ mature T$_{reg}$ derived from CD69$^+$ OTII (n = 10) or OTIIx*Lta*$^{-/-}$ (n = 9) CD4$^+$ thymocytes co-cultured with OVA$_{323-339}$-loaded mTEC (**g**), mTEC^{lo} or mTEC^{hi} (n = 5 for OTII and OTIIx*Lta*$^{-/-}$) (**h**) after 5 days. Data are pooled from three (**g**) and two (**h**) independent experiments. **i** Flow cytometry profiles and fold change in the frequencies of CD25$^+$Foxp3$^+$ mature T$_{reg}$ derived from CD69$^+$ OTII CD4$^+$ thymocytes pretreated (n = 7) or not (n = 8) with the blocking LTβR-Fc receptor after 5 days of co-culture. Data are pooled from two independent experiments. **j** T$_{reg}$ conversion assay: OVA$_{323-339}$-loaded mTEC were co-cultured with CD25$^+$ T$_{reg}$P or Foxp3^{lo} T$_{reg}$P from RipmOVAxOTIIxFoxp3^{eGFP} mice. T$_{reg}$P were pretreated or not with the blocking LTβR-Fc receptor. **k**, **l** Flow cytometry profiles (**k**) and fold change in the frequencies of mature T$_{reg}$ (**l**) derived from the conversion of pretreated or not CD25$^+$ T$_{reg}$P or Foxp3^{lo} T$_{reg}$P after 72 h or 24 h of co-culture, respectively (n = 7 from two independent experiments). **m** Relative expression of *Il4* and *Rela* in co-cultures of OVA$_{323-339}$-loaded mTEC and CD69$^+$ semi-mature OTII or OTIIx*Lta*$^{-/-}$ CD4$^+$ thymocytes (n = 9 from two independent experiments). **n** Fold change in the frequencies of CD25$^+$Foxp3$^+$ mature T$_{reg}$ derived from CD69$^+$ OTII or OTIIx*Lta*$^{-/-}$ CD4$^+$ thymocytes co-cultured with OVA$_{323-339}$-loaded mTEC with (n = 6) or without (n = 10) a neutralizing anti-IL4 antibody. Data are pooled from two independent experiments. Error bars show mean ± SEM, *p < 0.05, **p < 0.01, ***p < 0.001 and ****p < 0.0001 using unpaired two-tailed Mann–Whitney U test for (**a**), (**g**–**i**) and (**l**), unpaired two-tailed Student's t test for (**d**), (**f**) and (**m**) and Kruskal–Wallis test for (**n**). Source data are provided as a Source Data File.

that of CD25$^+$ T$_{reg}$P decreased with CD69$^+$ CD4$^+$ from OTIIx*Lta*$^{-/-}$ mice compared to OTII mice. Moreover, blocking LTα$_1$β$_2$-LTβR interactions using the soluble LTβR-Fc receptor, also resulted in an increased Foxp3^{lo} T$_{reg}$P conversion and a decreased CD25$^+$ T$_{reg}$P conversion (Fig. 9e, f), indicating that the lymphotoxin axis limits the Foxp3^{lo} T$_{reg}$P developmental pathway in favor of the CD25$^+$ T$_{reg}$P pathway. As previously reported[42], mTEC had the capacity to induce antigen-specific CD25$^+$Foxp3$^+$ mature T$_{reg}$ after 5 days of co-culture (Fig. 9g). We found a higher conversion in CD25$^+$Foxp3$^+$ mature T$_{reg}$ when OVA$_{323-339}$-loaded mTEC were co-cultured with CD69$^+$CD4$^+$ SP thymocytes from OTIIx*Lta*$^{-/-}$ mice compared to OTII mice. A similar enhanced T$_{reg}$ generation was observed irrespective of the mTEC maturation state (Fig. 9h). Moreover, blocking LTα$_1$β$_2$-LTβR interactions, also resulted in an increased mature T$_{reg}$ conversion after 5 days of co-culture (Fig. 9i). These results show that LTα$_1$β$_2$-LTβR interactions with mTEC act as a negative regulator of CD25$^+$Foxp3$^+$ mature T$_{reg}$ conversion via the Foxp3^{lo} T$_{reg}$P developmental pathway. To further define whether the LTα$_1$β$_2$-LTβR axis controls the conversion of Foxp3^{lo} T$_{reg}$P into CD25$^+$Foxp3$^+$ mature T$_{reg}$, we backcrossed RipmOVAxOTIIx*Rag2*$^{-/-}$ mice with the Foxp3^{eGFP} reporter mice, which allowed us to purified both T$_{reg}$P. We performed antigen-specific co-culture assays using OVA$_{323-339}$-loaded mTEC with CD25$^+$ or Foxp3^{lo} T$_{reg}$P purified from RipmOVAxOTIIxFoxp3^{eGFP} mice and treated them or not with the soluble LTβR-Fc receptor (Fig. 9j and Supplementary Fig. 12). The addition in the co-culture of LTβR-Fc receptor caused a greater conversion into CD25$^+$Foxp3$^+$ mature T$_{reg}$ by Foxp3^{lo} T$_{reg}$P, but not by CD25$^+$ T$_{reg}$P (Fig. 9k, l). Altogether, these data reveal that the LTα$_1$β$_2$-LTβR axis acts as a feedback mechanism by which T$_{reg}$P can limit their own differentiation.

We next evaluated whether the LTα$_1$β$_2$-LTβR axis regulates *Il4* expression in mTEC in these co-culture assays. Interestingly, we found higher levels of *Il4* in OVA$_{323-339}$-loaded mTEC co-cultured with CD69$^+$CD4$^+$ SP thymocytes from OTIIx*Lta*$^{-/-}$ compared to OTII mice, demonstrating that *Lta* negatively regulates the expression of *Il4* in mTEC (Fig. 9m). Consistently, *Rela* was also higher in co-cultures with CD69$^+$CD4$^+$ SP thymocytes from OTIIx*Lta*$^{-/-}$ mice. To test the hypothesis that *Il4* overexpression observed in the absence of *Lta* may be responsible for the enhanced conversion of CD69$^+$CD4$^+$ SP thymocytes into mature T$_{reg}$ (Fig. 9g), we used a neutralizing anti-IL-4 antibody in these co-culture assays. Strikingly, the increased conversion of CD69$^+$CD4$^+$ SP thymocytes from OTIIx*Lta*$^{-/-}$ mice into CD25$^+$Foxp3$^+$ T$_{reg}$ was fully abolished by IL-4 neutralization (Fig. 9n). Overall, these results demonstrate that the LTα$_1$β$_2$-LTβR axis negatively regulates CD25$^+$Foxp3$^+$ T$_{reg}$ conversion by repressing IL-4 expression in mTEC.

Discussion

Recent advances have revealed that CD25$^+$Foxp3$^+$ mature T$_{reg}$ arise from two distinct developmental pathways involving CD25$^+$ and Foxp3^{lo} T$_{reg}$P[7,14,15,48]. Although the CD25$^+$ T$_{reg}$P pathway is well studied, the more recently identified Foxp3^{lo} T$_{reg}$P pathway remains poorly investigated. Our study reveals that the LTα$_1$β$_2$-LTβR axis plays an unexpected role in limiting CD25$^+$Foxp3$^+$ T$_{reg}$ generation via the Foxp3^{lo} T$_{reg}$P developmental pathway.

Previous reports have found that the first step of T$_{reg}$ development is linked to the TCR signal strength, implicating transcription factors of the Nr4a family[49]. Concomitantly to TCR signaling, CD28 costimulation promotes T$_{reg}$ generation by inducing Foxp3 expression[8]. We observed that *Cd28*$^{-/-}$ mice have decreased numbers of both CD25$^+$ T$_{reg}$P and Foxp3^{lo} T$_{reg}$P, resulting in a drastic reduction of mature T$_{reg}$. Our data show that the stimulation of TCR and CD28 also upregulates the expression of LTα$_1$β$_2$ in CD25$^+$ T$_{reg}$P and Foxp3^{lo} T$_{reg}$P. In addition to TCR/CD28 signals, γ-chain cytokines are important regulators of T$_{reg}$ development since *Il2*$^{-/-}$ and *Il15*$^{-/-}$ mice exhibit a severe reduction of T$_{reg}$P and mature T$_{reg}$ in their thymus[10,50]. Interestingly, we found that IL-2 controls LTα$_1$β$_2$ expression specifically in mature T$_{reg}$. Accordingly, LTα$_1$β$_2$ and CD25 levels were tightly correlated and IL-2 in vitro stimulation led to a dose-dependent LTα$_1$β$_2$ upregulation in mature T$_{reg}$. A recent report described that IL-2 also increases LTα$_1$β$_2$ expression in peripheral T$_{reg}$[51], suggesting a conserved regulatory mechanism between the thymus and the periphery.

Although Foxp3^{lo} T$_{reg}$P leads to the generation of CD25$^+$Foxp3$^+$ T$_{reg}$ upon intrathymic transfer[14,15], the underlying mechanisms that control this newly identified developmental pathway remain unknown. The generation of Foxp3^{eGFP}x*Lta*$^{-/-}$ mice revealed that *Lta* expression limits T$_{reg}$ development from Foxp3^{lo} T$_{reg}$P. To our knowledge, LTα is the first identified molecule that fine-tunes the Foxp3^{lo} T$_{reg}$P developmental pathway. Although CD25$^+$ T$_{reg}$P express LTα$_1$β$_2$ to some extent, these cells remain poorly affected compared to Foxp3^{lo} T$_{reg}$P in Foxp3^{eGFP}x*Lta*$^{-/-}$ mice. We show that the increased cellularity of Foxp3^{lo} T$_{reg}$P and mature T$_{reg}$ in Foxp3^{eGFP}x*Lta*$^{-/-}$ mice was likely a direct consequence of enhanced proliferation and survival. Moreover, given that LTβR signaling was found to regulate the expression of chemokines involved in thymocyte trafficking[17] and that the LTα$_1$β$_2$- LTβR axis has been implicated in T$_{reg}$ trafficking in a model of pancreatic islet allograft[18,52], future investigations are expected to clarify whether *Lta*-deficiency could affect the intrathymic migration of T$_{reg}$ subsets. Multiparametric flow cytometry analyses based on maturational markers revealed an unexpected heterogeneity in both T$_{reg}$P and mature T$_{reg}$. Our results highlight that CD25$^+$ T$_{reg}$P is a highly heterogenous

population, with cells at distinct maturational stages. Compared to CD25$^+$ T_{reg}P, Foxp3^{lo} T_{reg}P contain more mature cells at M1 and M2 stages, similarly to CD25$^+$Foxp3$^+$ mature T_{reg}. Our transcriptomic and flow cytometry analyses highlight that CD25$^+$ T_{reg}P and Foxp3^{lo} T_{reg}P subsets contain not only precursors but also CD62L$^+$ mature cells, which is a reliable marker for cells about to leave the thymus[53]. Therefore, cells commonly called T_{reg}P likely contain cells with the ability to emigrate, although this requires further investigations. The CD69$^+$CD62L$^-$ Foxp3^{lo} T_{reg}P population, displaying a mature phenotype characterized by high levels of H2K^b and Qa2, increased in Foxp3^{eGFP}x*Lta*$^{-/-}$ mice, suggesting that this putative transitional stage towards mature T_{reg} is regulated by *Lta*. Altogether, our data identified LTα as a negative regulator of T_{reg} maturational development.

A recent study performed scRNA-seq on thymic T_{reg} using presorted subpopulations from TCliβxTCRα$^{+/-}$xFoxp3^{GFP} mice and characterized CD25$^+$$T_{reg}$P, Foxp3^{lo}$T_{reg}$P and mature de novo T_{reg}[54]. In contrast, our cell-sorting strategy based on the entire T_{reg} lineage allowed us to also capture CD122$^+$ pre-T_{reg}P and transitional T_{reg} states from Foxp3^{eGFP} and Foxp3^{eGFP}x*Lta*$^{-/-}$ mice. Moreover, we characterized the metabolic profile in our scRNA-seq experiment during T_{reg} development, which remained unknown to date. Interestingly, whereas CD25$^+$ T_{reg}P rely on both glucose and OXPHOS mitochondrial dependencies, our transcriptomic and functional metabolic analyses revealed that like mature T_{reg}, Foxp3^{lo} T_{reg}P are highly dependent on OXPHOS activity and have a lower dependency on glucose metabolism. These findings are consistent with the fact that CD25$^+$ T_{reg}P and Foxp3^{lo} T_{reg}P have a distinct transcriptomic profile[15,54]. In Foxp3^{eGFP}x*Lta*$^{-/-}$ mice, the glucose dependency substantially increased in both T_{reg}P and mature T_{reg}, indicating that *Lta* regulates their metabolic profile. This higher glucose dependency may be linked to the enhanced survival and/or proliferation of T_{reg}P and mature T_{reg} observed in Foxp3^{eGFP}x*Lta*$^{-/-}$ mice. Further investigations will elucidate whether the distinct metabolic profiles of CD25$^+$ T_{reg}P and Foxp3^{lo} T_{reg}P depend on their responsiveness to γ-chain cytokines and influence their epigenetic landscape. Understanding the intricate interplay between the two T_{reg}P and their respective stromal niches, which could modulate their metabolic profiles and influence their differentiation, represents an exciting area for future research.

T_{reg} conversion assays using co-cultures of CD69$^+$ semi-mature OTII CD4$^+$ SP thymocytes with mTEC that express LTβR revealed that the $LT\alpha_1\beta_2$-LTβR axis acts as a negative regulator of CD25$^+$Foxp3$^+$ mature T_{reg} conversion. We found an enhanced generation of Foxp3^{lo} T_{reg}P from CD69$^+$ CD4$^+$ SP thymocytes in the absence of *Lta* in CD4$^+$ SP thymocytes or when $LT\alpha_1\beta_2$-LTβR interactions were blocked with the soluble LTβR-Fc receptor. In line with these observations, this resulted in an increased conversion into CD25$^+$Foxp3$^+$ mature T_{reg}. Furthermore, T_{reg} conversion assays using co-cultures with T_{reg}P showed that the $LT\alpha_1\beta_2$-LTβR axis acts as an inhibitory feedback by which Foxp3^{lo} T_{reg}P can limit their own differentiation into CD25$^+$Foxp3$^+$ mature T_{reg}. In agreement with a previous study[15], we found that Foxp3^{lo} T_{reg}P express higher levels of IL-4Rα than CD25$^+$ T_{reg}P both by scRNA-seq and flow cytometry. Moreover, Foxp3^{lo} T_{reg}P have a higher ability to respond to IL-4 stimulation than CD25$^+$ T_{reg}P. Remarkably, *Il4* expression was higher in *Lta*$^{-/-}$ mice, which correlated with a greater frequency of Eomes$^+$ memory-like CD8$^+$ SP thymocytes and phospho-Stat6$^+$ cells. In vivo IL-4 neutralization resulted in a substantial reduction of Foxp3^{lo} T_{reg}P and CD25$^+$Foxp3$^+$ mature T_{reg} whereas CD25$^+$ T_{reg}P were over-represented, indicating that IL-4 favors the Foxp3^{lo} T_{reg}P pathway at the expense of the CD25$^+$ T_{reg}P developmental pathway. Future studies are expected to define the respective contribution of T_{reg}P and mature T_{reg} in $LT\alpha_1\beta_2$-controlled IL-4 production by mTEC.

ScRNA-seq, qPCR and IL-4^{eGFP} reporter mice revealed that mTEC are a valuable source of IL-4 in addition to NKT2. Strikingly, mTEC produced a larger amount of IL-4 upon antigen-specific co-cultures with CD69$^+$CD4$^+$ SP thymocytes purified from OTIIx*Lta*$^{-/-}$ mice compared to OTII mice, indicating that *Lta* expression negatively regulates *Il4* expression in mTEC. This higher production correlated with a greater conversion into mature T_{reg}, which was abrogated by a neutralizing IL-4 antibody. The classical NF-κB member p65 has the ability to bind to the P4/PRE-I and P1 sites of the *Il4* promoter and upregulate its transcription[41,55]. Whereas the non-classical NF-κB pathway is preferentially activated by lymphotoxin signaling at steady state[27,56], our data indicate a preferential usage of the classical NF-κB pathway characterized by an upregulation of p65 when lymphotoxin signaling is disrupted. Since IL-4 is regulated by the classical NF-κB member p65, which was overexpressed in *Lta*$^{-/-}$ mice, this cytokine upregulation in *Lta*$^{-/-}$ mice is likely induced by the classical NF-κB pathway. Interestingly, previous studies have shown that IL-4 acts as a proliferation and survival factor of peripheral T_{reg}[57–59]. Thus, IL-4 may not only induce mature T_{reg} conversion but also promote their survival and proliferation. In line with this hypothesis, we found reduced expression of the pro-apoptotic protein BIM in Foxp3^{lo} T_{reg}P and mature T_{reg} of Foxp3^{eGFP}x*Lta*$^{-/-}$ mice. Whereas IL-2 is crucial for the CD25$^+$ T_{reg}P developmental pathway[10,50], our findings show that IL-4 preferentially regulates the Foxp3^{lo} T_{reg}P developmental pathway, indicating that these two cytokines play a non-overlapping role in T_{reg} development. IL-15, also implicated in T_{reg} development, is expressed by mTEC[10,12,14]. Therefore, by their ability to produce both IL-15 and IL-4, mTEC likely constitute a privilege niche that controls T_{reg} development.

In summary, this study shows that instructive signals of the "two step model" induce the gradual upregulation of the membrane-bound $LT\alpha_1\beta_2$ during T_{reg} development. Importantly, we identify that $LT\alpha_1\beta_2$-LTβR interactions act as an inhibitory checkpoint that limits the Foxp3^{lo} T_{reg}P developmental pathway by negatively regulating IL-4 production in mTEC (Supplementary Fig. 13). Interestingly, human thymi, routinely removed during pediatric cardiac surgery, constitute a novel source of stable T_{reg} for cell therapy that can be purified in large quantities[60,61]. Given that CD25$^+$ and Foxp3^{lo} T_{reg} P-derived T_{reg} likely exhibit a differential ability to protect against distinct autoimmune disorders[15,62], targeting $LT\alpha_1\beta_2$-LTβR interactions may therefore be used to foster the Foxp3^{lo} T_{reg}P pathway in order to treat specific pathologies. Our findings are, thus, expected to pave the way for therapeutic strategies tailored to treat distinct autoimmune and inflammatory disorders.

Methods

Mice

All mice - CD45.1, CD45.2 and CD45.1/2 WT (Charles River), CD45.2 *Lta*$^{-/-}$[63], *Rag2*$^{-/-}$[64], *Cd28*$^{-/-}$[65], OTII[66], Rip-mOVA[67], CD45.1 Foxp3^{eGFP}[68], *Rag2*^{GFP19}, *Foxp3*$^{Thy1.120}$, *Il15*^{KO}[69] and *Il2*^{KO} (B6.129P2-Il2tm1Hor/J, JAX laboratories) - were on a pure C57BL/6 background. The IL-4^{eGFP} reporter (4get) mice[70] were on a C57BL/6 or BALB/c background. CD45.2 *Lta*$^{-/-}$ mice were backcrossed with CD45.1 Foxp3^{eGFP} mice (CD45.1 Foxp3^{eGFP}x*Lta*$^{-/-}$ mice). OTII mice were backcrossed on a *Rag2*$^{-/-}$ background (OTIIx*Rag2*$^{-/-}$ mice) and OTIIx*Rag2*$^{-/-}$ on a *Lta*$^{-/-}$ background (OTIIx*Rag2*$^{-/-}$x*Lta*$^{-/-}$ mice). Rip-mOVA mice were backcrossed with OTIIx*Rag2*$^{-/-}$ mice (Rip-mOVAxOTIIx*Rag2*$^{-/-}$). Rip-mOVAxOTIIx*Rag2*$^{-/-}$ were backcrossed with Foxp3^{eGFP} mice (Rip-mOVAxOTIIxFoxp3^{eGFP}). *Foxp3*$^{Thy1.1}$ mice were backcrossed with *Rag2*^{GFP} mice (*Rag2*^{GFP}x*Foxp3*$^{Thy1.1}$ mice) and *Rag2*^{GFP}x*Foxp3*$^{Thy1.1}$ mice on a *Il15*^{KO} or *Il2*^{KO} background (*Il15*^{KO}x*Rag2*^{GFP}x*Foxp3*$^{Thy1.1}$ or *Il2*^{KO}x*Rag2*^{GFP}x*Foxp3*$^{Thy1.1}$ mice). All mice were maintained under specific pathogen free conditions at the CIML (Marseille, France). Mice were housed under a standard 12 h/12 h light-dark cycle, with a controlled ambient temperature of 22 °C ± 2 °C, and relative humidity between 45% and 65%. Standard food and water were given *ad libitum*. For all experiments, male and female mice were sex- and

age-matched. Unless specified, adult mice were used between 6 and 8 weeks of age. Chimeras were generated between 6 and 12 weeks of age. All experiments were done in accordance with National and European laws for laboratory animal welfare (EEC Council Directive 2010/63/UE) and approved by the Marseille Ethical Committee for Animal Experimentation no.14.

Bone marrow chimeras

Bone marrow chimeras were generated by co-injecting intravenously (i.v.) 2×10^6 BM cells from CD45.2 WT mice with 2×10^6 BM cells from either CD45.1 Foxp3^{eGFP} or Foxp3^{eGFP}x*Lta*$^{-/-}$ mice (ratio 1:1) into lethally irradiated CD45.1/2 WT recipients (two doses of 500 rads, 12 h apart, X-ray using a RS-2000 Irradiator, Rad Source Technologies). Similarly, 5×10^6 BM cells from CD45.1 Foxp3^{eGFP} mice were injected into lethally irradiated CD45.2 WT or *Lta*$^{-/-}$ recipients. Mice were analyzed 6 weeks post-reconstitution.

Thymic cell isolation

For T_{reg} isolation, thymi were mechanically dissociated on a 70 μm cell strainer. CD4$^+$ SP thymocytes were pre-enriched by depleting CD8$^+$ and CD11c$^+$ cells using biotinylated anti-CD8α (clone 53.6.7; Biolegend) and anti-CD11c (clone N418; Biolegend) antibodies with anti-biotin microbeads and ran on an AutoMACS Pro separator using the Deplete program (Miltenyi Biotec). For TEC isolation, thymi were digested 10 min at 37 °C in HBSS medium containing 50 μg/ml of Liberase™ (Roche) and 100 μg/ml DNase I (Roche) and were then subjected to vigorous pipetting. This step was repeated until complete tissue digestion. Cells were filtered through a 70 μm strainer to remove clumps. CD45$^+$ hematopoietic cells were depleted using biotinylated anti-CD45 antibodies (clone 30-F11; Biolegend) with anti-biotin microbeads, and run on an AutoMACS Pro separator using the DepleteS program (Miltenyi Biotec). CD69$^+$CD4$^+$ SP thymocytes, T_{reg}P, mature T_{reg}, NKT, and mTEC subsets were cell-sorted using a FACSAria III cell sorter (BD Biosciences).

In vivo IL-4 neutralization experiments

Lta$^{-/-}$ neonates received an i.p. injection of either isotype control (clone RTK2071, Biolegend) or neutralizing anti-mouse IL-4 antibody (clone 11B11, BioXcell) on the day they were born (100 μg) and 3 days later (100 μg). Mice were analyzed 5 days post-birth.

In vitro antigen-specific T_{reg} conversion assays

Co-culture assays between mTEC and CD69$^+$CD4$^+$ SP thymocytes to assess T_{reg} conversion were performed[71]. Briefly, 1×10^3 cell-sorted total mTEC (CD45$^-$EpCAM$^+$Ly51^{lo}UEA-1^{hi}), mTEC^{hi} (CD45$^-$EpCAM$^+$Ly51^{lo}UEA-1^{hi}CD80$^+$) and mTEC^{lo} (CD45$^-$EpCAM$^+$Ly51^{lo}UEA-1^{hi}CD80$^-$) from WT thymi were loaded or not for 90 min with $OVA_{323\text{-}339}$ peptide (5 μg/ml, PolyPeptide) at 37 °C. Cells were then co-cultured with 5×10^3 purified CCR6$^-$CD25$^-$CD69$^+$CD4$^+$CD8$^-$ SP thymocytes from OTIIx*Rag2*$^{-/-}$ mice pre-incubated or not during 1 h at 37 °C with recombinant LTβR-Fc (2 μg/ml, RnD systems) or from OTIIx*Rag2*$^{-/-}$x*Lta*$^{-/-}$ mice in a complete medium containing D-MEM (ThermoFisher Scientific), 10 % FBS (Sigma Aldrich), 2 mM L-glutamine, 1 mM sodium pyruvate, 2.10^{-5} M 2-mercaptoethanol, 100 IU/ml penicillin, and 100 μg/ml streptomycin (all from ThermoFisher Scientific). In addition, total mTEC were co-cultured with 5×10^3 purified CD25$^+$ T_{reg}P or Foxp3^{lo} T_{reg}P from Rip-mOVAxOTIIxFoxp3^{eGFP} mice pre-incubated or not during 1 h at 37 °C with recombinant LTβR-Fc (2 μg/ml, RnD systems). Alternatively, 10 μg/mL of neutralizing anti-mouse IL-4 antibody (clone 11B11, BioXcell) was added in the co-cultures of $OVA_{323–339}$-loaded mTEC with CCR6$^-$CD25$^-$CD69$^+$CD4$^+$CD8$^-$ SP from OTIIx*Rag2*$^{-/-}$ or OTIIx*Rag2*$^{-/-}$x*Lta*$^{-/-}$ mice. The conversion into CD25$^+$ T_{reg}P, Foxp3^{lo} T_{reg}P, or CD25$^+$Foxp3$^+$ mature T_{reg} was analyzed by flow cytometry 18 h, 24 h, 72 h, or 5 days later, as indicated in the legends.

In vitro T_{reg}P conversion assays with IL-4 stimulation

1×10^4 purified CD25$^+$ T_{reg}P or Foxp3^{lo} T_{reg}P from Foxp3^{eGFP} mice were incubated in complete RPMI medium supplemented with different doses of mouse IL-4 (0.5, 1 or 100 ng/mL; Peprotech). After 72 h, cells were harvested, stained with anti-CD4 and anti-CD25 antibodies, and analyzed by flow cytometry for the conversion into CD25$^+$Foxp3^{eGFP+} mature T_{reg}.

In vitro activation of T_{reg} cell subsets

For CD3ε stimulation, 2×10^4 purified CD25$^+$ T_{reg}P, Foxp3^{lo} T_{reg}P or CD25$^+$Foxp3$^+$ T_{reg} from Foxp3^{eGFP} mice were cultured with different doses (0.1, 1, 2.5 or 5 μg/mL) of coated anti-CD3ε antibody (clone 2C11, BD Biosciences) in a complete RPMI medium containing soluble anti-CD28 antibody (0.5 μg/mL, clone 37.51, Biolegend) in the presence of a low dose of IL-2 (5 ng/mL, Immunotools). For IL-2 stimulation, 2×10^4 purified CD25$^+$ T_{reg}P, Foxp3^{lo} T_{reg}P, or mature T_{reg} from Foxp3^{eGFP} mice were cultured with a low dose of coated anti-CD3ε antibody (2 μg/mL, clone 2C11, BD Biosciences) in a complete RPMI medium containing soluble anti-CD28 antibody (0.5 μg/mL, clone 37.51, Biolegend) in the presence or not of different doses (5, 20 or 40 ng/mL) of IL-2 (Immunotools). After 16 h, cells were harvested and analyzed for $LT\alpha_1\beta_2$ expression by flow cytometry.

Flow cytometry

Cells were stained with standard procedures using antibodies listed in Supplementary Data 1. For intracellular staining, cells were fixed, permeabilized, and stained with the Foxp3 staining kit according to the manufacturer's instructions (ThermoFisher Scientific). Fluorescence minus one (FMO) and secondary antibody controls were used to set positive staining gates. NKT cells were detected using CD1d tetramers loaded with PBS-57 or unloaded (obtained from the National Institutes of Health Tetramer Core Facility). For $LT\alpha_1\beta_2$ staining, cells were incubated with LTβR-Fc ($1\ \mu g/10^6$ cells, R&D systems) for 45 min on ice, and staining was visualized using an APC-conjugated donkey anti-human IgG $F(ab')_2$ antibody (Jackson ImmunoResearch). For all panels, we inferred the background levels observed in the respective cell subsets from *Lta*$^{-/-}$ mice. To evaluate mitochondrial activity, thymocytes were stained with MitoTracker Deep Red (100 nM) (Thermo Fisher) for 30 min at 37 °C in complete RPMI medium. For unbiased clustering of the cells from the T_{reg} lineage, data from all samples were concatenated and analyzed using the t-SNE plugin of the FlowJo software (BD Life Sciences, version 10.8.1). The PhenoGraph plugin was used for the unsupervised discrimination of T_{reg} subsets (with a k-nearest neighbor value of 130 for Fig. 3i and 120 for Fig. 4f), which were then visualized on the t-SNE dimensional reduction and quantified. The color code representing the expression level of each marker in heatmaps was normalized on the median intensity value for a given marker. Levels of $LT\alpha_1\beta_2$ expression were measured in thymic T_{reg} subsets from *Rag2*^{GFP}x*Foxp3*$^{Thy1.1}$ (Fig. 1b–f), *Rag2*^{GFP}x*Foxp3*$^{Thy1.1}$x*Il15*$^{-/-}$ and *Rag2*^{GFP}x*Foxp3*$^{Thy1.1}$x*Il2*$^{-/-}$ (Fig. 2d, e) mice on a BD LSR Fortessa at Infinity (Toulouse, France). The other flow cytometry experiments were conducted using FACSCanto II, BD LSR II, and Symphony cytometers (BD Biosciences) at CIML (Marseille, France). Data were analyzed using the FlowJo software (BD Life Sciences).

SCENITH™ metabolic profiling

SCENITH kit containing all reagents (including anti-puromycin, clone R4743L-E8) and protocols were obtained (www.scenith.com) and the T_{reg} metabolic profile was analyzed[35]. Briefly, 4×10^6 thymocytes were plated at 40×10^6 cells/ml in complete medium in a 96-well plate and treated with Puromycin (10 μg/mL) and DMSO (Co), 2-deoxy-glucose (2DG; 100 mM), oligomycin (O; 1 μM), a combination of 2DG and oligomycin (DGO) or harringtonine (H; 2 μg/mL) for 40 min at 37 °C, 5 % CO_2. Cells were washed in cold FACS buffer and incubated with a BD

Horizon™ Fixable Viability Stain 700 (BD Biosciences). Then, cells were stained with primary-conjugated antibodies for 25 min at 4 °C in FACS Buffer and were fixed and permeabilized with the Foxp3 staining kit according to the manufacturer's instructions (ThermoFisher Scientific). Intracellular staining with anti-puromycin and anti-Foxp3 antibodies was performed by incubating cells during 1 h at 4 °C in Permeabilization Buffer (ThermoFisher Scientific).

Immunofluorescence staining

20-µm-thick-frozen thymic sections embedded in O.C.T (Sakura Finetek) were stained[72]. Briefly, sections were fixed with 2% paraformaldehyde (Merck), saturated with 3% BSA, and 0.01 % Triton X100 in 0.1 M Tris HCl buffer. Sections were then stained for 45 min with anti-keratin 14 and anti-NK1.1 Alexa Fluor 647 (clone PK136, Biolegend) in hybridization buffer (1% BSA and 0.02% Triton X100 in 0.1 M Tris-HCl, pH 7.4). Keratin 14 staining was revealed with a Cy3-conjugated anti-rabbit antibody (ThermoFisher Scientific). Sections were counterstained with DAPI (1 µg/mL; Biolegend) and mounted with Mowiol (Calbiochem). Confocal microscopy was performed with an LSM 880 confocal microscope (Carl Zeiss Microscopy) and analysed using Zen Blue (3.5.093).

RT-qPCR

Total RNA was isolated with TRIzol (ThermoFisher Scientific) and cDNA was synthesized with random oligo-dT primers and Superscript II reverse transcriptase (ThermoFisher Scientific). qPCR was performed with SYBR Premix Ex Taq master mix (Takara) on an ABI 7500 fast real-time PCR system (Applied Biosystem). Reactions were conducted in duplicates. Results were normalized to *Actin* mRNA. Primer sequences are provided in Supplementary Data 2.

scRNA-seq library preparation

CD8- and CD11c-depleted thymocytes from Foxp3^{eGFP} and Foxp3^{eGFP}x*Lta*$^{-/-}$ mice were stained with fluorescently labeled antibodies (Fig. 5a) and barcoded using TotalSeq-A antibodies (BioLegend). FACS sorted Live Dead$^-$CD4$^+$CD8$^-$CCR6$^-$CD3ε$^+$ expressing either CD25, Foxp3^{eGFP}, or both were pooled and subsequently prepared for single-cell sequencing using the Chromium Single Cell 3′ kit v3 (10X Genomics) with a targeted number of 10,000 total cells. Libraries were prepared according to the manufacturer's instructions. The concentration and quality of cDNA libraries were respectively determined using the Qubit dsDNA HS Assay Kit (ThermoFisher Scientific) for the Qbit fluorometer and the High Sensitivity DNA Analysis Kit (Agilent) for the bioanalyzer. Libraries were sequenced on the Illumina NextSeq2000 sequencer.

Data analysis for scRNA-seq analysis

mRNA and Cell Hashing FASTQ raw files were processed using Cell Ranger v6.0.1 (10X genomics Inc.) software with default parameters to perform alignment, filtering, barcode counting, and unique molecular identifier (UMI) counting. Reads were aligned to the mm10 genome. A total number of 4,798 cells were identified with a mean of 44,015 reads per cell and a median of 1,992 genes per cell. Data sets were analysed using the R package Seurat 4.0.5[73]. First, cells were demultiplexed (with the Cell Hashing tags) to their original sample groups using the *HTODemux* function from Seurat R package with automated threshold finding to define the best quantile. 302 doublet cells and 4 negative cells were identified and removed. Quality control (QC) was performed to remove poor quality cells. We observed co-variables using the ShIVA interface and set the following thresholds[74]: cells with less than 603 or more than 4128 detected genes, cells with less than 851 or more than 21,686 detected UMI, cells with more than 9.94% mitochondrial gene expression, and cells with less than 11.5% ribosomal gene expression were removed. Expression data was normalized using the *NormalizeData* function of the Seurat R package (logNormalize method and scale factor of 10,000). We centered the expression data from these factors using the Seurat R package *ScaleData* function (centering true and scaling false).

Feature selection was performed using the Seurat R package *FindVariableGene* function; the variance-stabilizing transform (vst) algorithm and 2,000 genes were selected. Principal component analysis (PCA) was ran using Seurat *RunPCA* function on those 2,000 most variable genes. UMAP dimensionality reduction was ran using Seurat *RunUMAP* function on the first 50 principal components from PCA. Clustering was done with Seurat *FindClusters* based on the first 30 principal components from PCA dimensionality reduction and with an initial resolution parameter set to 1.1. Markers for each cluster were identified using Wilcoxon Rank Sum test from Seurat *FindAllMarkers* with the log fold change threshold of 0.1 and an adjusted FDR threshold of 0.001. Cell-cycle scores and cell phases were calculated using *CellCycleScoring* with s.genes and g2m.genes from the *Seurat* package. After cell type analysis using marker genes, we identified several clusters to be contaminants, in proliferation or recirculating cells and excluded them. PCA, UMAP, and clustering (with resolution 0.8) were performed again on the filtered dataset.

Heatmaps of gene expression data per cluster were created using the *Heatmap* function of the ComplexHeatmap (v2.10.0)[75] R package. Expression was presented as the mean of the expression of cells inside each cluster. Values were scaled to make them more comparable. Module scores of gene set list from the KEGG database were calculated using the *AddModuleScore* function from the Seurat R package. The Nebulosa package was used to visualize features on UMAP embeddings using kernel density estimation[76].

Trajectory analysis were performed using Monocle 3[32]. Cells were clustered using the Monocle 3 *cluster_cells* function with a resolution set to 0.003. Trajectories were computed using the Monocle 3 *learn_graph* and *order_cells* function. Gene set scores were computed as previously described and plotted along the pseudotime trajectories. All regression lines were computed using the ggplot2 *geom_smooth* function, setting the method to "loess".

Statistical analysis

All statistical analyses were performed in GraphPad Prism 9.5.1 and were considered statistically different at a p-value < 0.05. Unpaired Student's t test, Mann–Whitney U test, one-way ANOVA, or Kruskal–Wallis test were calculated. Normal distribution of the data was assessed using d'Agostino-Pearson omnibus normality test. Correlation was calculated using the parametric two-tailed Pearson correlation test or the non-parametric two-tailed Spearman correlation test. Statistical comparison of module scores between conditions for each cluster was performed using the Wilcoxon test with Benjamini-Hochberg multitest correction. *p < 0.05; **p < 0.01; ***p < 0.001, ****p < 0.0001. Error bars represent mean ± SEM.

Reporting summary

Further information on research design is available in the Nature Portfolio Reporting Summary linked to this article.

Data availability

The scRNA-seq data generated in this study have been deposited in the GEO database under accession number GSE237589. All data supporting the findings of this study are found within the paper and its Supplementary Information. Source data are provided with this paper.

Code availability

Scripts used to analyze sequencing data have been deposited on GitHub (https://github.com/CIML-bioinformatic/MIlab_LTaTreg-Thymus) and Zenodo (https://doi.org/10.5281/zenodo.12705747)[77].

References

1. Fontenot, J. D., Dooley, J. L., Farr, A. G. & Rudensky, A. Y. Developmental regulation of Foxp3 expression during ontogeny. *J. Exp. Med.* **202**, 901–906 (2005).
2. Aschenbrenner, K. et al. Selection of Foxp3$^+$ regulatory T cells specific for self antigen expressed and presented by Aire+ medullary thymic epithelial cells. *Nat. Immunol.* **8**, 351–358 (2007).
3. Perry, J. S. A. et al. Distinct contributions of Aire and antigen-presenting-cell subsets to the generation of self-tolerance in the thymus. *Immunity* **41**, 414–426 (2014).
4. Charaix, J. et al. Recirculating Foxp3+ regulatory T cells are restimulated in the thymus under Aire control. *Cell. Mol. Life Sci.* **79**, 355 (2022).
5. Lio, C. W. J. & Hsieh, C. S. A two-step process for thymic regulatory T cell development. *Immunity* **28**, 100–111 (2008).
6. Klein, L., Robey, E. A. & Hsieh, C. S. Central CD4$^+$ T cell tolerance: deletion versus regulatory T cell differentiation. *Nat. Rev. Immunol.* **19**, 7–18 (2019).
7. Santamaria, J. C., Borelli, A. & Irla, M. Regulatory T cell heterogeneity in the thymus: impact on their functional activities. *Front Immunol.* **12**, 1–8 (2021).
8. Tai, X., Cowan, M., Feigenbaum, L. & Singer, A. CD28 costimulation of developing thymocytes induces Foxp3 expression and regulatory T cell differentiation independently of interleukin 2. *Nat. Immunol.* **6**, 152–162 (2005).
9. Mahmud, S. A. et al. Costimulation via the tumor-necrosis factor receptor superfamily couples TCR signal strength to the thymic differentiation of regulatory T cells. *Nat. Immunol.* **15**, 473–481 (2014).
10. Apert, C. et al. IL-2 and IL-15 drive intrathymic development of distinct periphery-seeding CD4+Foxp3+ regulatory T lymphocytes. *Front Immunol.* **13**, 965303 (2022).
11. Hemmers, S. et al. IL-2 production by self-reactive CD4 thymocytes scales regulatory T cell generation in the thymus. *J. Exp. Med.* **216**, 2466–2478 (2019).
12. Cui, G. et al. Characterization of the IL-15 niche in primary and secondary lymphoid organs in vivo. *Proc. Natl Acad. Sci. USA* **111**, 1915–1920 (2014).
13. Tai, X. et al. Foxp3 transcription factor is proapoptotic and lethal to developing regulatory T cells unless counterbalanced by cytokine survival signals. *Immunity* **38**, 1116–1128 (2013).
14. Marshall, D., Sinclair, C., Tung, S. & Seddon, B. Differential requirement for IL-2 and IL-15 during bifurcated development of thymic regulatory T cells. *J. Immunol.* **193**, 5525–5533 (2014).
15. Owen, D. L. et al. Thymic regulatory T cells arise via two distinct developmental programs. *Nat. Immunol.* **20**, 195–205 (2019).
16. Gommerman, J. L. & Browning, J. L. Lymphotoxin/LIGHT, lymphoid microenvironments and autoimmune disease. *Nat. Rev. Immunol.* **3**, 642–655 (2003).
17. Borelli, A. & Irla, M. Lymphotoxin: from the physiology to the regeneration of the thymic function. *Cell Death Differ.* **28**, 2305–2314 (2021).
18. Brinkman, C. C. et al. Treg engage lymphotoxin beta receptor for afferent lymphatic transendothelial migration. *Nat. Commun.* **7**, 12021 (2016).
19. Yu, W. et al. Continued RAG expression in late stages of B cell development and no apparent re-induction after immunization. *Nature* **400**, 682–687 (1999).
20. Liston, A. et al. Differentiation of regulatory Foxp3 T cells in the thymic cortex. *Proc. Natl Acad. Sci. USA* **105**, 11903–11908 (2008).
21. McCaughtry, T. M., Wilken, M. S. & Hogquist, K. A. Thymic emigration revisited. *J. Exp. Med.* **204**, 2513–2520 (2007).
22. Thiault, N. et al. Peripheral regulatory T lymphocytes recirculating to the thymus suppress the development of their precursors. *Nat. Immunol.* **16**, 628–634 (2015).
23. Yang, E. J., Zou, T., Leichner, T. M., Zhang, S. L. & Kambayashi, T. Both retention and recirculation contribute to long-lived regulatory T-cell accumulation in the thymus. *Eur. J. Immunol.* **44**, 2712–2720 (2014).
24. Moran, A. E. et al. T cell receptor signal strength in Treg and iNKT cell development demonstrated by a novel fluorescent reporter mouse. *J. Exp. Med.* **208**, 1279–1289 (2011).
25. Apert, C., Romagnoli, P. & van Meerwijk, J. P. M. IL-2 and IL-15 dependent thymic development of Foxp3-expressing regulatory T lymphocytes. *Protein Cell* **9**, 322–332 (2018).
26. Bayer, A. L., Lee, J. Y., de la Barrera, A., Surh, C. D. & Malek, T. R. A function for IL-7R for CD4$^+$CD25$^+$Foxp3$^+$ T regulatory cells. *J. Immunol.* **181**, 225–234 (2008).
27. Lopes, N., Charaix, J., Cédile, O., Sergé, A. & Irla, M. Lymphotoxin α fine-tunes T cell clonal deletion by regulating thymic entry of antigen-presenting cells. *Nat. Commun.* **9**, 1–16 (2018).
28. Bouillet, P. et al. BH3-only Bcl-2 family member Bim is required for apoptosis of autoreactive thymocytes. *Nature* **415**, 922–926 (2002).
29. Gray, D. H. D. et al. The BH3-Only proteins bim and puma cooperate to impose deletional tolerance of organ-specific antigens. *Immunity* **37**, 451–462 (2012).
30. Irla, M. et al. Three-dimensional visualization of the mouse thymus organization in health and immunodeficiency. *J. Immunol.* **190**, 586–596 (2013).
31. Schuster, M., Plaza-Sirvent, C., Visekruna, A., Huehn, J. & Schmitz, I. Generation of Foxp3$^+$CD25$^-$ regulatory T-cell precursors requires c-rel and IκBNS. *Front Immunol.* **10**, 1583 (2019).
32. Cao, J. et al. The single-cell transcriptional landscape of mammalian organogenesis. *Nature* **566**, 496–502 (2019).
33. Shi, H. & Chi, H. Metabolic control of treg cell stability, plasticity, and tissue-specific heterogeneity. *Front Immunol.* **10**, 2716 (2019).
34. Newton, R., Priyadharshini, B. & Turka, L. A. Immunometabolism of regulatory T cells. *Nat. Immunol.* **17**, 618–625 (2016).
35. Argüello, R. J. et al. SCENITH: a flow cytometry-based method to functionally profile energy metabolism with single-cell resolution. *Cell Metab.* **32**, 1063–1075.e7 (2020).
36. Xing, Y., Wang, X., Jameson, S. C. & Hogquist, K. A. Late stages of T cell maturation in the thymus involve NF-κB and tonic type i interferon signaling. *Nat. Immunol.* **17**, 565–573 (2016).
37. Lee, Y. J., Holzapfel, K. L., Zhu, J., Jameson, S. C. & Hogquist, K. A. Steady-state production of IL-4 modulates immunity in mouse strains and is determined by lineage diversity of iNKT cells. *Nat. Immunol.* **14**, 1146–1154 (2013).
38. Lai, D. et al. KLF13 sustains thymic memory-like CD8+ T cells in BALB/c mice by regulating IL-4-generating invariant natural killer T cells. *J. Exp. Med.* **208**, 1093–1103 (2011).
39. Wang, H. et al. Myeloid cells activate iNKT cells to produce IL-4 in the thymic medulla. *Proc. Natl Acad. Sci. USA* **116**, 22262–22268 (2019).
40. Zhou, T. A. et al. Thymic macrophages consist of two populations with distinct localization and origin. *Elife* **11**, e75148 (2022).
41. Li-Weber, M., Giasi, M. & Krammer, P. H. Involvement of Jun and Rel proteins in up-regulation of interleukin-4 gene activity by the T cell accessory molecule CD28. *J. Biol. Chem.* **273**, 32460–32466 (1998).
42. Wirnsberger, G., Mair, F. & Klein, L. Regulatory T cell differentiation of thymocytes does not require a dedicated antigen-presenting cell but is under T cell-intrinsic developmental control. *Proc. Natl Acad. Sci. USA* **106**, 10278–10283 (2009).
43. Malchow, S. et al. Aire enforces immune tolerance by directing autoreactive T cells into the regulatory T cell lineage. *Immunity* **44**, 1102–1113 (2016).
44. Malchow, S. et al. Aire-dependent thymic development of tumor-associated regulatory T cells. *Science* **339**, 1219–1224 (2013).
45. Michelson, D. A., Hase, K., Kaisho, T., Benoist, C. & Mathis, D. Thymic epithelial cells co-opt lineage-defining transcription factors to eliminate autoreactive T cells. *Cell* **185**, 2542–2558.e18 (2022).

46. Wells, K. L. et al. Combined transient ablation and single cell RNA sequencing reveals the development of medullary thymic epithelial cells. *Elife* **9**, 1–80 (2020).
47. Jin, S. et al. Inference and analysis of cell-cell communication using CellChat. *Nat. Commun.* **12**, 1088 (2021).
48. Irla, M. Instructive Cues of Thymic T Cell Selection. *Annu. Rev. Immunol.* **26**, 95–119 (2022).
49. Sekiya, T. et al. Nr4a receptors are essential for thymic regulatory T cell development and immune homeostasis. *Nat. Immunol.* **14**, 230–237 (2013).
50. Fontenot, J. D., Rasmussen, J. P., Gavin, M. A. & Rudensky, A. Y. A function for interleukin 2 in Foxp3-expressing regulatory T cells. *Nat. Immunol.* **6**, 1142–1151 (2005).
51. Piao, W. et al. Regulatory T cells condition lymphatic endothelia for enhanced transendothelial migration. *Cell Rep.* **30**, 1052–1062.e5 (2020).
52. Saxena, V. et al. Treg tissue stability depends on lymphotoxin beta-receptor- and adenosine-receptor-driven lymphatic endothelial cell responses. *Cell Rep.* **39**, 110727 (2022).
53. James, K. D. et al. Endothelial cells act as gatekeepers for LTβRdependent thymocyte emigration. *J. Exp. Med.* **215**, 2984–2993 (2018).
54. Owen, D. L., Rue, R. S., La, Munro, S. A. & Farrar, M. A. Tracking regulatory T cell development in the thymus using single-cell RNA sequencing/TCR sequencing. *J. Immunol.* **209**, 1300–1313 (2022).
55. Li-Weber, M. & Krammer, P. H. Regulation of IL4 gene expression by T cells and therapeutic perspectives. *Nat. Rev. Immunol.* **3**, 534–543 (2003).
56. Irla, M., Hollander, G. & Reith, W. Control of central self-tolerance induction by autoreactive CD4+ thymocytes. *Trends Immunol.* **31**, 71–79 (2010).
57. Pandiyan, P. & Lenardo, M. J. The control of $CD4^+CD25^+Foxp3^+$ regulatory T cell survival. *Biol. Direct* **3**, 6 (2008).
58. Zhou, J. Y., Alvarez, C. A. & Cobb, B. A. Integration of il-2 and il-4 signals coordinates divergent regulatory T cell responses and drives therapeutic efficacy. *Elife* **10**, 1–27 (2021).
59. Yang, W. C. et al. Interleukin-4 supports the suppressive immune responses elicited by regulatory T cells. *Front. Immunol.* **8**, 1508 (2017).
60. Dijke, I. E. et al. Discarded human thymus is a novel source of stable and long-lived therapeutic regulatory T cells. *Am. J. Transplant.* **16**, 58–71 (2016).
61. Bernaldo-de-Quirós, E. et al. First-in-human therapy with Treg produced from thymic tissue (thyTreg) in a heart transplant infant. *J. Exp. Med.* **220**, e20231045 (2023).
62. Wyss, L. et al. Affinity for self antigen selects Treg cells with distinct functional properties. *Nat. Immunol.* **17**, 1093–1101 (2016).
63. De Togni, P. et al. Abnormal development of peripheral lymphoid organs in mice deficient in lymphotoxin. *Science.* **264**, 703–707 (1994).
64. Shinkai, Y. et al. RAG-2-deficient mice lack mature lymphocytes owing to inability to initiate V(D)J rearrangement. *Cell* **68**, 855–867 (1992).
65. Morin, S. O. et al. In the absence of its cytosolic domain, the CD28 molecule still contributes to T cell activation. *Cell. Mol. Life Sci.* **72**, 2739–2748 (2015).
66. Barnden, M. J., Allison, J., Heath, W. R. & Carbone, F. R. Defective TCR expression in transgenic mice constructed using cDNA- based α- and β-chain genes under the control of heterologous regulatory elements. *Immunol. Cell Biol.* **76**, 34–40 (1998).
67. Kurts, C. et al. Constitutive class i-restricted exogenous presentation of self antigens in vivo. *J. Exp. Med.* **184**, 923–930 (1996).
68. Wang, Y. et al. Th2 lymphoproliferative disorder of lat Y136F mutant mice unfolds independently of TCR-MHC engagement and is insensitive to the action of $Foxp3^+$ regulatory T cells. *J. Immunol.* **180**, 1565–1575 (2008).
69. Kennedy, M. K. et al. Reversible defects in natural killer and memory CD8 T cell lineages in interleukin 15-deficient mice. *J. Exp. Med.* **191**, 771–780 (2000).
70. Mohrs, M., Shinkai, K., Mohrs, K. & Locksley, R. M. Analysis of type 2 immunity in vivo with a bicistronic IL-4 reporter. *Immunity* **15**, 303–311 (2001).
71. Borelli, A., Zamit, C. & Irla, M. Medullary thymic epithelial cell antigen-presentation assays. *Bio Protoc.* **13**, e4865 (2023).
72. Sergé, A., Bailly, A. L., Aurrand-Lions, M., Imhof, B. A. & Irla, M. For3D: Full organ reconstruction in 3D, an automatized tool for deciphering the complexity of lymphoid organs. *J. Immunol. Methods* **424**, 32–42 (2015).
73. Hao, Y. et al. Integrated analysis of multimodal single-cell data. *Cell* **184**, 3573–3587.e29 (2021).
74. Aussel, R. et al. ShIVA: a user-friendly and interactive interface giving biologists control over their single-cell RNA-seq data. *Sci. Rep.* **13**, 14377 (2023).
75. Gu, Z., Eils, R. & Schlesner, M. Complex heatmaps reveal patterns and correlations in multidimensional genomic data. *Bioinformatics* **32**, 2847–2849 (2016).
76. Alquicira-Hernandez, J. & Powell, J. E. Nebulosa recovers single-cell gene expression signals by kernel density estimation. *Bioinformatics* **37**, 2485–2487 (2021).
77. Spinelli, L. CIML-bioinformatic/MIlab_LTaTreg-Thymus: article publication release. *Zenodo* https://doi.org/10.5281/zenodo.12705747 (2024).

Acknowledgements

We are grateful to Jacques Nunes and Geoffrey Guittard (CRCM, Marseille, France) for providing us with *Cd28*$^{-/-}$ mice, to Bernard Malissen (CIML, Marseille, France) for $Foxp3^{eGFP}$ mice, to Joost P.M. van Meerwijk (Inifinity, Toulouse, France) for *Rag2*^{GFP}x*Foxp3*$^{Thy1.1}$, *Il2*$^{-/-}$ and *Il15*$^{-/-}$ mice and to David Voehringer and Andreas Ruhl (FAU, Erlangen, Germany) for 4get mice. We also thank the National Institutes of Health Tetramer Facility for PBS57:CD1d tetramers. We thank the CIML animal facility, flow cytometry, PICSL imaging facility (ImagImm), and Genomics platform for technical support. We are grateful to Benoit Salomon (Infinity, Toulouse, France), Lena Alexopoulou (CIML, Marseille, France), and Arnauld Sergé (LAI, Marseille, France) for helpful discussions. We thank Serge van de Pavert (CIML, Marseille, France) for help in preparing the Supplementary Fig. 13. This work was supported by the ARC Foundation (PJA20171206491 to M.I.), Inserm CoPoC—proof of concept (N° MAT-PI-17326-A-01 to M.I.), Agence de Biomédecine (21GREFFE009 to M.I.) and the Agence Nationale de la Recherche (grant ANR-22-CE18-0045-01 Reality to M.I.). This work was supported by the France Génomique national infrastructure, funded as part of the "Investissements d'Avenir" program managed by the Agence Nationale de la Recherche (contract ANR-10-INBS-0009). We also acknowledge financial support from n° ANR-10-INBS-04-01 France Bio Imaging. A.B. was supported by a PhD fellowship from the Ministère de l'Enseignement Supérieur et de la Recherche et de l'Innovation (MESRI) and by the Fondation ARC pour la Recherche sur le Cancer (ARCDOC42022010004424). The Supplementary Fig. 13 was created with BioRender.com.

Author contributions

A.B., J.C.S, C.A., C.Z., and M.I. conducted the experiments, analyzed and interpreted the data. L.S. and J.C. analyzed scRNA-seq data. R.J.A. provided assistance with data interpretation, discussion on SCENITH and scRNA-seq data and reviewed the manuscript. P.P. provided us anti-puromycin antibody. A.B., J.C.S., and M.I. wrote the manuscript. M.I. initiated, supervised, and conceived the study.

Competing interests

The authors declare the existence of a financial/non financial competing interest. M.I. holds a patent related to Treg genetically modified for the lymphotoxin alpha gene (PCT/EP2020/063346; WO2020229546A1). There are restrictions to the commercial use of SCENITH™ due to pending patent application (PCT/EP2020/060486;WO2020212362A1 to R.J.A.). All other authors declare no competing interests.

Additional information

Supplementary information The online version contains supplementary material available at https://doi.org/10.1038/s41467-024-51164-5.

Correspondence and requests for materials should be addressed to Magali Irla.

Peer review information *Nature Communications* thanks Derk Amsen and the other anonymous reviewers for their contribution to the peer review of this work. A peer review file is available.